

Gap-gradient methods for solving generalized mixed integer inverse optimization: an application to political gerrymandering

Ari Smith

Department of Industrial and Systems Engineering, University of Wisconsin-Madison, ajsmith44@wisc.edu

Justin J. Boutilier

Telfer School of Management, University of Ottawa, boutilier@telfer.uottawa.ca

Inverse optimization has received much attention in recent years, but little literature exists for solving generalized mixed integer inverse optimization. We propose a new approach for solving generalized mixed-integer inverse optimization problems based on sub-gradient methods. We characterize when a generalized inverse optimization problem can be solved using sub-gradient methods and we prove that modifications to classic sub-gradient algorithms can return exact solutions in finite time. Our best implementation improves solution time by up to 90% compared to the best performing method from the literature. We then develop custom heuristic methods for graph-based inverse problems using a combination of graph coarsening and ensemble methods. Our heuristics are able to further reduce solution time by up to 52%, while still producing near-optimal solutions. Finally, we propose a new application domain – quantitatively identifying gerrymandering – for generalized inverse integer optimization. We apply our overall solution approach to analyze the congressional districts of the State of Iowa using real-world data. We find that the accepted districting marginally improves population imbalance at the cost of a significant increase in partisan efficiency gap. We argue that our approach can produce a more nuanced data-driven argument that a proposed districting should be considered gerrymandered.

Key words: Inverse Mixed Integer Optimization, Multi-Objective Optimization, Political Districting

1. Introduction

Inverse optimization (IO) has received significant attention in recent years; see Chan et al. (2023) for a thorough review. At a high level, inverse optimization infers unknown parameters (e.g., cost vector, constraint matrix, etc.) of a *forward optimization problem* (FOP) such that an observed solution is rendered optimal (or nearly optimal) for the FOP. Inverse optimization has been applied to a wide range of problems including radiation therapy (Chan et al. 2014), transportation (Patriksson 2015), and cellular biology (Zhao et al. 2015).

The IO literature can be partitioned into two general approaches, depending on the problem setting. The first approach (“classical IO”) is to assume that the observed solution is optimal for the FOP and then leverage results from duality theory to design an appropriate IO problem (Ahuja and Orlin 2001, Schaefer 2009). The second approach (“generalized IO”) is to make no assumptions about the optimality of the observed solution (i.e., it may not be optimal or even feasible) and then use a loss function to design an appropriate IO problem (Chan et al. 2014).

To date, most of the IO literature has focused on convex FOPs with relatively little research on purely integer or mixed-integer FOPs. In the context of integer IO problems, there are two streams of literature. First, Schaefer (2009) and Lamperski and Schaefer (2015) characterize the polyhedral representation of purely integer and mixed-integer IO problems, respectively. Second, Wang (2009) propose a cutting plane approach for efficiently solving mixed-integer IO problems. Recent research has extended this cutting plane approach to be more efficient using parallel computing (Wang 2013) or trust regions (Bodur et al. 2022), and to solve generalized mixed-integer IO problems (Moghaddass and Terekhov 2020).

In this paper, we propose a new approach for solving generalized mixed-integer IO problems based on sub-gradient methods. Our method leverages the observation that the generalized IO problem is equivalent to minimizing a loss function over a bounded domain and many commonly used loss functions permit sub-gradient calculation. We present the conditions for when a generalized IO problem can be solved using sub-gradient methods and we test various implementations, including gradient descent and the Frank-Wolfe method.

1.1. Motivating example: political gerrymandering

In the United States of America, representation in federal and state legislatures is apportioned by democratic elections in geographic sub-regions known as legislative districts. Every 10 years, a nationwide census is conducted and the data gathered is used to redraw new legislative districts. This redrawing process, commonly referred to as *political districting*, is regulated by federal and state laws. The United States Constitution requires that political districts must be of equal population, and state constitutions enforce additional requirements upon district design. For example, the state of Iowa requires that congressional districts do not split up counties (Iowa Constitution Article III §37) and that districts must be as compact as practicable (Iowa State Code, Chapter 42.4.4).

Political districting is often politically contentious, as there are frequent allegations – in high-profile court cases and in the broader public political sphere – that districts are drawn to create imbalanced voting power across populations (Lieb 2022, Villeneuve 2022, Sherman 2019). When such imbalance is used to privilege the representation of one political party over another, it is referred to as *partisan gerrymandering*. Allegations of partisan gerrymandering often result in trials, where judges are tasked with deciding if a particular political districting is illegal, and as such must be redrawn. In these cases, the judicial system has indicated a desire for quantitative methods of measuring partisan gerrymandering, allowing for judicial rulings to be made with more confidence (and based on defensible data) (Vieth v. Jubelirer 2004). However, quantitatively identifying gerrymandering is challenging because public and judicial discourse around gerrymandering

typically invokes common sense notions — particularly of *fairness* and *compactness* — which are often not quantified or critically elaborated.

The foundation of quantitative methods for identifying political gerrymandering relies on the development of district-level metrics that quantify and align with sociopolitical values; either those legally required (e.g., compactness in many states) or those in the public discourse (e.g., “fair” representation). Two constitutional requirements – contiguity and equal population – are easily quantified. However, a frequent third requirement – compactness – has been subject to much debate. For example, Young (1988) demonstrated that the common sense notions of compactness should not be expected to match a single quantitative metric, because nearly (if not) all compactness metrics can be met with counterexamples that are quantitatively compact but do not feel compact to qualitative perceptions, or vice versa. Similarly, “fair” partisan representation has been quantified with a multitude of metrics, under such names as partisan bias (Grofman and King 2007), competitiveness of elections (Nagle 2017), and the efficiency gap of wasted votes (Stephanopoulos and McGhee 2015).

Initial research on identifying political gerrymandering invoked hard cutoffs for a single (chosen) metric as an indicator of gerrymandering (Stephanopoulos and McGhee 2015). However, a univariate approach fails to consider the contingency of what values are actually attainable for real political geographies of state populations, or that a multitude of competing metrics may inhibit each other from simultaneously meeting some benchmark, even if they all align with different democratic values that are important to courts. To address this shortcoming, researchers have used computational methods to develop Markov Chain Monte Carlo approaches that create a set of “reasonable districtings” and corresponding probability distributions for each districting metric. A proposed political districting is then compared against this information to determine whether or not it is a statistical outlier; if so, this may indicate that a districting prioritizes an undemocratic value and should be considered gerrymandering (Duchin et al. 2019, Daryl DeFord and Solomon 2020).

In this paper, we propose an inverse optimization approach to quantitatively identify partisan gerrymandering. By formulating the process of drawing political districtings as a multi-objective optimization problem, inverse optimization allows us to consider how a proposed districting enacts a prioritization of some values over others with respect to what is possible in a given political geography. Thus, even if metrics that are motivated to track some notion of partisan unfairness are deemed fictitious or not a compelling legal argument in themselves, an inverse optimization analysis may show that a districting prioritizes unfairness specifically to the detriment of other constitutionally mandated objectives, such as creating compact districts or reducing population imbalance. We argue that this approach can produce a more nuanced data-driven argument that a proposed districting should be considered gerrymandered.

1.2. Contributions

We summarize our contributions as follows:

1. We propose a new approach – *gap-gradient methods* – for generalized inverse integer optimization that leverages the problem’s similarity to minimizing a bounded convex function where querying the function gradient is computationally difficult. We characterize when a generalized IO problem can be solved using sub-gradient methods and we prove that modifications to classic sub-gradient algorithms can return exact solutions in finite time. We evaluate our methods using a set of instances from the MIPLIB 2017 library and we find that our best implementation is able to improve solution time by up to 90%, compared to the best performing method from the literature.
2. We develop a custom heuristic method for graph-based inverse problems using a combination of coarsening methods from the field of graph partitioning and ensemble methods from the field of machine learning. Our methods use ensembles of smaller problem instances to produce approximate solutions that provably converge towards the optimal inverse solution as ensemble size increases, while saving computational expense and allowing for tractable run times for large real-world problems. Our heuristic is able to reduce the median solution time by 52%, while still producing near-optimal solutions.
3. We propose a new application domain – quantitatively identifying gerrymandering – for generalized inverse integer optimization. We apply our overall solution approach to analyze the congressional districts of the State of Iowa using real-world data. We show that accepted and previously rejected district plans both greatly prioritize minimizing population imbalance over district compactness or partisan efficiency gap. However, the increased priority on population imbalance in the accepted district plan results in a 16% decrease in population imbalance while creating a 372% increase in partisan efficiency gap compared to the rejected plan.

Many of the graph-based IO methods formulated and implemented in this paper (Contribution 2) can also be used in several other applications, such as flexible job shop scheduling, employee scheduling, and facility location, particularly in settings where there are competing objectives to be considered (e.g., distribution of polling locations).

2. Literature Review

Our work contributes to three primary streams of literature: inverse optimization (Section 2.1), optimization approaches for political districting (Section 2.2), and quantitative methods for identifying gerrymandering (Section 2.3).

2.1. Inverse Optimization

The idea of IO was proposed by Ahuja and Orlin (2001) who studied linear FOPs in a classical IO setting. Since then, there has been much research on IO, including for conic FOPs (Iyengar and Kang 2005), general convex FOPs (Zhang and Xu 2010), purely integer FOPs (Schaefer 2009), and mixed-integer FOPs (Wang 2009, Bulut and Ralphs 2021). See Chan et al. (2023) for a recent review.

In recent years, there have been several extensions to IO, often inspired by machine learning and data-driven optimization. Importantly, Chan et al. (2014) developed the generalized IO paradigm, where no assumptions are made about the optimality or feasibility of the observed solutions. Other extensions include IO with multiple observations (Keshavarz et al. 2011, Babier et al. 2021), IO with uncertain data (Ghobadi et al. 2018, Aswani et al. 2018), and goodness of fit measures for IO (Chan et al. 2019).

Our work is most closely related to the IO literature where the FOP is a mixed-integer linear program. In this vein, Wang (2009) proposed the first algorithmic approach (a cutting plane algorithm) for solving mixed integer IO problems. Since then, there have been several extensions that seek to improve tractability (Bodur et al. 2022, Moghaddass and Terekhov 2020, Wang 2013). Most similar to our paper is the work of Moghaddass and Terekhov (2020) who develop the first approach for generalized inverse mixed integer optimization by leveraging Wang (2009)’s cutting plane method, while assuming a loss function where the optimality gap is formulated as an absolute gap. Recently (and in parallel to this work), Scroccaro et al. (2023) develop descent methods for learning solutions to mixed integer IO problems. However, they use a more general augmented suboptimality loss function that does not necessarily permit provable finite time convergence to the optimal solution.

We contribute to this literature in three key ways: (i) we propose a new solution method for solving generalized inverse multi-objective mixed integer optimization in finite time that uses first order methods of minimizing a bounded convex function, (ii) we propose a set of heuristic approaches inspired by ensemble methods in machine learning that are tailored to the setting where the FOP is graph-based (i.e., amenable to graph coarsening), and (iii) we propose a new and potentially impactful application domain for generalized inverse integer optimization.

2.2. Optimization approaches to political districting

Political districting has a long history as an optimization problem in the operations research community. See Ricca et al. (2013) or Swamy et al. (2022) for a recent literature review. The literature in this area typically uses mixed-integer programming to design political districtings (Hess et al. 1965). Most approaches focus on nonpolitical metrics such as population imbalance, contiguity,

and compactness (Garfinkel and Nemhauser 1970). Since these problems are very computationally challenging, research has focused on developing efficient formulations and both exact and heuristic solution methods (Mehrotra et al. 1998, Validi et al. 2022).

More recently, researchers have developed districting models that include or optimize for notions of political fairness such as efficiency gap, partisan symmetry, and competitiveness (Swamy et al. 2022, King et al. 2015). For example, Swamy et al. (2022) produce a formulation that considers districting design as a multi-objective optimization problem between district compactness and variety of fairness-related metrics, and uses the formulation to explore the Pareto frontier of tradeoffs between pairs of metrics over a state’s political geography. While we do not directly contribute another districting formulation, we make minor modifications to Swamy et al. (2022)’s formulation and their multi-objective approach, and use it as the FOP for our generalized inverse optimization model, demonstrating another use of their formulation.

2.3. Quantitative Methods for Identifying Gerrymandering

Initial research on identifying political gerrymandering invoked hard cutoffs for a single (chosen) metric as an indicator of gerrymandering; see Stephanopoulos and McGhee (2018) for a review. In recent years, research has focused on how metrics can quantitatively identify gerrymandering using approaches that are not cutoff rules. For example, Duchin (2018) propose the use of Markov Chain Monte Carlo methods to produce a set of reasonable districtings. This set of districtings is then used to create statistical distributions of particular partisan fairness (or compactness) metrics. If the districting under scrutiny presents a partisan fairness metric that is a strong statistical outlier compared to the distribution, then an argument can be made that the districting explicitly prioritizes disproportionate representation (i.e., partisan “unfairness”). Note that this line of argument requires the assumption that the constructed set of districtings accurately represents average or permissible districtings. These methods have been applied to the study of various underlying metrics for district design, including partisan seat share (Duchin et al. 2019), partisan symmetry (Daryl DeFord and Solomon 2020), and proportion of majority-minority districts (Becker et al. 2021).

In contrast to previous approaches, we contribute a new method for quantitatively measuring how district design impacts partisan fairness. Rather than comparing a districting to a constructed distribution of permissible districtings like the Markov Chain Monte Carlo methods, our inverse optimization methods analyze how a district compares to the boundary of what is feasible, while critically recognizing that multiple metrics can be in competition with each other. For example, if a districting that meets a certain benchmark for one metric limits the best possible performance on other metrics, then producing judgements based on the evaluation of a single metric may be

unhelpful when multiple metrics are valued. With inverse optimization, we can understand how a districting choice enacts a prioritization of metrics and their corresponding democratic values. For example, if one argued that high political unfairness is not sufficient to disqualify a districting, then one may show that the districting under scrutiny prioritizes political unfairness explicitly to the detriment of another legal right, such as district compactness or population balance. We believe our approach may provide a more robust argument that a districting should be disqualified.

3. Models

In this section, we introduce the general structure of the forward multi-objective mixed-integer linear optimization problem (Section 3.1) and the corresponding inverse optimization problem (Section 3.2)

3.1. The Forward Problem

To apply inverse optimization, we must first define the structure of the forward optimization problem (FOP). Inverse optimization implicitly assumes that the observed solutions were generated by a decision making process similar to the FOP. In the context of political districting, the decision making process is typically represented by a multi-objective mixed-integer linear optimization problem (Swamy et al. 2022).

We first introduce the general problem structure and provide the specific FOP for political districting in Section 6. Let $\mathbf{y} \in \mathbb{R}^n \times \mathbb{Z}^{n-q}$, $q = 0, 1, 2, \dots, n$ represent the decision variables for the FOP, and let $\mathbf{A} \in \mathbb{R}^{m \times n}$ and $\mathbf{b} \in \mathbb{R}^m$ represent the constraints. We let \mathcal{K} denote the set of objective functions. Then, the general multi-objective mixed-integer linear optimization problem can be written as

$$\underset{\mathbf{y}}{\text{minimize}} \quad \boldsymbol{\alpha}^T \mathbf{C} \mathbf{y} \tag{1a}$$

$$\text{subject to} \quad \mathbf{A} \mathbf{y} \leq \mathbf{b}, \tag{1b}$$

$$\mathbf{y} \in \mathbb{R}^n \times \mathbb{Z}^{n-q}, \tag{1c}$$

where the rows of $\mathbf{C} \in \mathbb{R}^{|\mathcal{K}| \times n}$ represent different linear objective functions and $\boldsymbol{\alpha} \in \mathbb{R}^{|\mathcal{K}|}$ denotes the cost vector. Let $\mathcal{S} = \{\mathbf{A} \mathbf{y} \leq \mathbf{b}, \mathbf{y} \in \mathbb{R}^n \times \mathbb{Z}^{n-q}\}$ denote the feasible region of the FOP, let $\mathcal{B}(\mathcal{S}) = \{\mathbf{C} \mathbf{y} \mid \mathbf{y} \in \mathcal{S}\}$ denote the set of feasible sub-objective values (also known as the FOP objective feasible space), and let $\mathcal{F}(\boldsymbol{\alpha}, \mathcal{S})$ represent the set of optimal solutions. Without loss of generality, we assume that \mathcal{S} is non-empty (Chan et al. 2014).

3.2. Inverse Optimization Model

In its classical form, inverse optimization seeks to, given a feasible region for a forward problem (\mathcal{S}) and an observed solution ($\hat{\mathbf{y}}$), return an objective function to the forward problem ($\bar{\alpha}$) for which the given solution is optimal – a property called *inverse feasibility* (Chan et al. 2023). Given a feasible solution to the forward problem, $\hat{\mathbf{y}} \in \mathcal{S}$, we let $\mathcal{C}(\hat{\mathbf{y}}, \mathcal{S}) = \{\alpha \in \mathbb{R}^{|\mathcal{K}|} \mid \hat{\mathbf{y}} \in \mathcal{F}(\alpha, \mathcal{S})\}$ denote the inverse-feasible region, which includes all cost vectors α that render $\hat{\mathbf{y}}$ optimal.

In data-driven contexts, it may not be reasonable to assume that $\hat{\mathbf{y}}$ is optimal for any possible objective (i.e., $\mathcal{C}(\hat{\mathbf{y}}, \mathcal{S}) = \emptyset$) or even feasible for the FOP (i.e., $\hat{\mathbf{y}} \notin \mathcal{S}$), so instead we seek to minimize some loss function of the forward objective that penalizes the extent to which inverse-feasibility is not satisfied. We denote the loss function $\ell(\hat{\mathbf{y}}, \mathcal{S}, \alpha)$, and note that if a solution $\hat{\mathbf{y}}$ does have some classically inverse feasible objective, then for any $\alpha \in \mathcal{C}(\hat{\mathbf{y}}, \mathcal{S})$, we have $\ell(\hat{\mathbf{y}}, \mathcal{S}, \alpha) = 0$. Chan et al. (2023) enumerate five possible loss functions that are useful in the data-driven inverse optimization context.

For any such loss function, the corresponding inverse optimization problem seeks to minimize the loss function, with constraints placed on the allowable objectives α , i.e., $\alpha \in \mathcal{A}$. We can write this problem as:

$$\begin{aligned} & \underset{\alpha}{\text{minimize}} && \ell(\hat{\mathbf{y}}, \mathcal{S}, \alpha) && (\text{GIO}(\hat{\mathbf{y}}, \mathcal{S})) \\ & \text{subject to} && \alpha \in \mathcal{A}. \end{aligned}$$

Many choices of loss functions have inverse optimization formulations that can be more practically expressed. For example, for the absolute sub-optimality loss function $\ell_{\text{ABS}}(\hat{\mathbf{y}}, \mathcal{S}, \alpha) = \alpha^\top \mathbf{C} \hat{\mathbf{y}} - \min_{\mathbf{y} \in \mathcal{S}} \alpha^\top \mathbf{C} \mathbf{y}$, which measures the difference in FOP objective value between the input $\hat{\mathbf{y}}$ and an optimal FOP solution for the given value of α , the equivalent inverse optimization formulation can be written as:

$$\begin{aligned} & \underset{\alpha, \xi_{\text{ABS}}}{\text{minimize}} && \xi_{\text{ABS}} && (\text{GIO}_{\text{ABS}}(\hat{\mathbf{y}}, \mathcal{S})) \\ & \text{subject to} && \alpha^\top \mathbf{C} \hat{\mathbf{y}} \leq \alpha^\top \mathbf{C} \mathbf{y} + \xi_{\text{ABS}}, \quad \forall \mathbf{y} \in \mathcal{S}, \\ & && \alpha \in \mathcal{A}. \end{aligned}$$

One potentially useful choice of \mathcal{A} for many applications is the unit simplex in dimension $|\mathcal{K}|$, because then α may be interpreted as a convex combination of weights for multiple objectives, allocating fractional amounts of importance to each objective in a form that adds up to 1. We also note that when C is the identity matrix, the generalized multi-objective inverse optimization problem $\text{GIO}(\hat{\mathbf{y}}, \mathcal{S})$ becomes a standard generalized inverse optimization problem, and all following solution approaches remain applicable without loss of generality.

4. Solution Approaches

In this section, we recap existing cutting plane methods (Section 4.1) and introduce a new approach for solving inverse mixed integer optimization problems (Section 4.2).

4.1. Cutting Planes

The first cutting plane algorithm for inverse mixed integer linear optimization was tailored to the classical inverse case that assumes the existence of an inverse-feasible objective (Wang 2009). The algorithm alternates between a master problem and a separation problem. The master problem produces an optimal forward problem objective (α) that is hypothesized to be inverse feasible (i.e., $\alpha \in \mathcal{C}(\hat{\mathbf{y}}, \mathcal{S})$) under partial knowledge of the forward feasible region (\mathcal{S}). The separation problem solves the forward optimization problem with the hypothesized objective (α) to produce an extreme point that can be added to the set \mathcal{S} . With each new extreme point that is added to \mathcal{S} , the set of potentially inverse-feasible objectives $\mathcal{C}(\hat{\mathbf{y}}, \mathcal{S})$ decreases in size. When the forward problem returns an extreme point that is already known to be in \mathcal{S} , further iterations will not remove elements from $\mathcal{C}(\hat{\mathbf{y}}, \mathcal{S})$, and so the output of the master problem is known to be an inverse-feasible solution. Thus, the algorithm returns the solution to the master problem and terminates. Since the forward problem is a mixed integer linear program, it is guaranteed to have a finite number of extreme points, and so the algorithm is guaranteed to (eventually) terminate.

More recently, Moghaddass and Terekhov (2020) proposed an extension to Wang’s algorithm that is suitable for data-driven generalized inverse optimization, in the case of an absolute sub-optimality loss function. As such, they use $\text{GIO}_{\text{ABS}}(\hat{\mathbf{y}}, \mathcal{S})$ as their master problem, and alternate between the master problem and the separation problem until an objective is found that minimizes the loss function. We present their algorithm structure (Algorithm 3) using our established notation in EC.7. In EC.2, we contribute a minor modification to the algorithm proposed by Moghaddass and Terekhov (2020) that utilizes the relative sub-optimality loss function, rather than absolute sub-optimality.

4.2. Gap-Gradient Methods

In this section, we describe our proposed solution methods – *gap-gradient methods* – and highlight various extensions. Our methods are applicable to a wide range of loss functions and constraint sets for the cost vector.

We first define what we call the *gap function* for a given generalized inverse optimization problem. The gap function is simply the loss function values over the feasible region of α , which we formally defined as follows.

DEFINITION 1 (GAP FUNCTION). For a generalized inverse optimization problem with fixed $\hat{\mathbf{y}}$ and \mathcal{S} , and some loss function $\ell(\hat{\mathbf{y}}, \mathcal{S}, \alpha)$, the gap function is defined as $\xi(\alpha) = \ell(\hat{\mathbf{y}}, \mathcal{S}, \alpha)$, $\forall \alpha \in \mathcal{A}$.

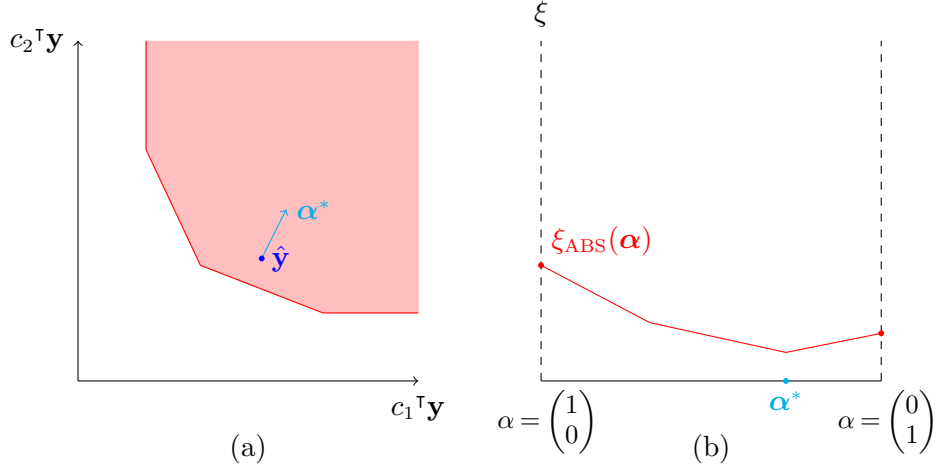


Figure 1 An example inverse optimization problem with two sub-objectives. (a) The FOP objective feasible space ($\text{conv}(\mathcal{B})$), inverse input ($\hat{\mathbf{y}}$), and the inverse solution (α^*), and (b) the corresponding absolute gap function (ξ_{ABS}) and its minimizer (α^*).

Note that the gap function will be a convex function as long as the loss function is a convex function of α , given fixed $\hat{\mathbf{y}}$ and \mathcal{S} . For the example where the loss function is absolute sub-optimality and α is constrained to the unit simplex, the gap function is $\xi_{ABS}(\alpha) = \alpha^\top \mathbf{C}\hat{\mathbf{y}} - \min_{\mathbf{y} \in \mathcal{S}} \alpha^\top \mathbf{C}\mathbf{y}$, where $\alpha \in \{\|\alpha\|_1 = 1, \alpha \geq 0\}$. To keep the rest of the paper succinct, all discussion henceforth concerns the case in which the loss function ℓ is absolute sub-optimality and the gap function domain \mathcal{A} is the unit simplex.

PROPOSITION 1. *The absolute gap function $\xi_{ABS}(\alpha)$ is a convex function.*

Proof of Proposition 1: First, note that the epigraph of $\xi_{ABS}(\alpha)$ is $\{\xi_{ABS} \in \mathbb{R} \mid \xi_{ABS} \geq \alpha^\top \mathbf{C}\hat{\mathbf{y}} - \min_{\mathbf{y} \in \mathcal{S}} \alpha^\top \mathbf{C}\mathbf{y}\}$, which is equivalent to $\{\xi_{ABS} \in \mathbb{R} \mid \xi_{ABS}(\alpha) \geq \alpha^\top \mathbf{C}\hat{\mathbf{y}} - \alpha^\top \mathbf{C}\mathbf{y}, \forall \mathbf{y} \in \mathcal{S}\}$. This space is the intersection of half-planes, and as such, is convex. Therefore, the gap function is a convex function because its epigraph is convex. \square

Figure 1 depicts an example inverse optimization problem with two sub-objectives, c_1 and c_2 . Figure 1(a) displays the convex hull of the set of feasible subobjective values for the forward problem ($\text{conv}(\mathcal{B})$), the inverse input ($\hat{\mathbf{y}}$), and the FOP multi-objective weighting (α^*) that minimizes the absolute sub-optimality loss function ℓ_{ABS} given $\hat{\mathbf{y}}$ and \mathcal{S} (i.e., the optimal inverse solution). Figure 1(b) displays the corresponding absolute gap function ($\xi_{ABS}(\alpha)$). The horizontal axis of Figure 1(b) describes the set of allowable multi-objective weightings for the two sub-objectives as a convex combination ranging from $\begin{pmatrix} 1 \\ 0 \end{pmatrix}$ to $\begin{pmatrix} 0 \\ 1 \end{pmatrix}$. Note that the vertices of $\text{conv}(\mathcal{B})$ correspond to the piecewise linear components of ξ , and that α^* (the solution to $\text{GIO}_{ABS}(\hat{\mathbf{y}}, \mathcal{S})$) is also the minimizer of $\xi_{ABS}(\alpha)$.

Now, consider the cutting plane algorithm used to solve GIO_{abs} (e.g., Moghaddass and Terekhov (2020)). At a given iteration k , we use $\boldsymbol{\alpha}^{(k)}$ to solve the FOP and obtain a solution $\mathbf{y}^{(k)}$ that is optimal for objective weighting $\boldsymbol{\alpha}^{(k)}$. Recall that $\mathcal{C}(\mathbf{y}^{(k)}, \mathcal{S})$ denotes the set of $\boldsymbol{\alpha}$ values that render $\mathbf{y}^{(k)}$ optimal for the FOP.

PROPOSITION 2. *If $\boldsymbol{\alpha}^{(k)} \in \mathcal{C}(\mathbf{y}^{(k)}, \mathcal{S})$, then $\xi_{\text{ABS}}(\boldsymbol{\alpha}^{(k)}) = \boldsymbol{\alpha}^{(k)\top} \mathbf{C}\hat{\mathbf{y}} - \boldsymbol{\alpha}^{(k)\top} \mathbf{C}\mathbf{y}^{(k)}$.*

Proof of Proposition 2: By the definition of the absolute sub-optimality loss function, $\xi_{\text{ABS}}(\boldsymbol{\alpha}^{(k)}) = \max_{\mathbf{y} \in \mathcal{S}} \boldsymbol{\alpha}^{(k)\top} \mathbf{C}\hat{\mathbf{y}} - \boldsymbol{\alpha}^{(k)\top} \mathbf{C}\mathbf{y}$. Since $\mathbf{y}^{(k)} = \arg \min_{\mathbf{y} \in \mathcal{S}} \boldsymbol{\alpha}^{(k)\top} \mathbf{C}\mathbf{y}$ by the definition of $\mathbf{y}^{(k)}$, it must be true that $\xi_{\text{ABS}}(\boldsymbol{\alpha}^{(k)}) = \max_{\mathbf{y} \in \mathcal{S}} \boldsymbol{\alpha}^{(k)\top} \mathbf{C}\hat{\mathbf{y}} - \boldsymbol{\alpha}^{(k)\top} \mathbf{C}\mathbf{y}^{(k)}$. \square

The implication of Proposition 2 is that we can efficiently query subgradients of the gap function, $\xi_{\text{ABS}}(\boldsymbol{\alpha}^{(k)})$. We demonstrate this via two cases. First, suppose that $\mathbf{y}^{(k)}$ is a vertex of $\text{conv}(\mathcal{B})$, then $\mathcal{C}(\mathbf{y}^{(k)}, \mathcal{S})$ is a closed convex subset of \mathcal{A} with dimension $\mathcal{K} - 1$ (by the definition of a vertex). For any $\boldsymbol{\alpha}$ in the interior of $\mathcal{C}(\mathbf{y}^{(k)}, \mathcal{S})$, the *gradient* of $\xi_{\text{ABS}}(\boldsymbol{\alpha})$ can be calculated as $\nabla(\boldsymbol{\alpha}^\top \mathbf{C}\hat{\mathbf{y}} - \boldsymbol{\alpha}^\top \mathbf{C}\mathbf{y}^{(k)}) = \mathbf{C}(\hat{\mathbf{y}} - \mathbf{y}^{(k)})$. Second, suppose that $\mathbf{y}^{(k)}$ is *not* a vertex of $\text{conv}(\mathcal{B})$. Then we note that $\xi_{\text{ABS}}(\boldsymbol{\alpha}^{(k)}) = \boldsymbol{\alpha}^{(k)\top} \mathbf{C}\hat{\mathbf{y}} - \boldsymbol{\alpha}^{(k)\top} \mathbf{C}\mathbf{y}^{(k)}$, and $\forall \boldsymbol{\alpha} \in \mathcal{A}$, $\xi_{\text{ABS}}(\boldsymbol{\alpha}) \geq \boldsymbol{\alpha}^\top \mathbf{C}\hat{\mathbf{y}} - \boldsymbol{\alpha}^\top \mathbf{C}\mathbf{y}^{(k)}$, since $\max_{\mathbf{y} \in \mathcal{S}} \boldsymbol{\alpha}^\top \mathbf{C}\hat{\mathbf{y}} - \boldsymbol{\alpha}^\top \mathbf{C}\mathbf{y} \geq \boldsymbol{\alpha}^\top \mathbf{C}\hat{\mathbf{y}} - \boldsymbol{\alpha}^\top \mathbf{C}\mathbf{y}^{(k)}$. Thus, the linear expression $\boldsymbol{\alpha}^\top \mathbf{C}\hat{\mathbf{y}} - \boldsymbol{\alpha}^\top \mathbf{C}\mathbf{y}^{(k)}$ defines a *subtangent plane* of $\xi_{\text{ABS}}(\boldsymbol{\alpha})$, and as such the gradient of the subtangent plane, $\nabla(\boldsymbol{\alpha}^\top \mathbf{C}\hat{\mathbf{y}} - \boldsymbol{\alpha}^\top \mathbf{C}\mathbf{y}^{(k)}) = \mathbf{C}(\hat{\mathbf{y}} - \mathbf{y}^{(k)})$ constitutes a *subgradient* of $\xi_{\text{ABS}}(\boldsymbol{\alpha})$.

REMARK 1. Suppose a generalized inverse optimization problem has a gap function $\xi(\boldsymbol{\alpha})$ that is convex, a gap function domain \mathcal{A} that is convex, and that the gap function is lower bounded over its domain. If it is possible to query a subgradient of $\xi(\boldsymbol{\alpha})$ for any $\boldsymbol{\alpha} \in \mathcal{A}$, then any subgradient method is guaranteed to converge towards the gap function minimizer as the number of iterations approaches infinity. Since we can query subgradients of $\xi_{\text{ABS}}(\boldsymbol{\alpha})$ at any $\boldsymbol{\alpha}^{(k)}$, we thus have the possibility of finding the gap function minimizer with any first-order method of minimizing convex functions over bounded domains.

Additional generalized inverse optimization scenarios that satisfy the conditions stated in Remark 1 include a relative sub-optimality loss function where \mathcal{A} is the unit simplex (Chan et al. 2023). See EC.3 for details on how our method applies to the relative sub-optimality loss function.

In general, subgradient methods do not necessarily guarantee finite-time convergence like the cutting plane method presented by Moghaddass and Terekhov (2020), which alternates solving relaxed master problems and generating cutting planes. For example, the descent-based methods developed by Scroccaro et al. (2023) are not guaranteed to converge upon loss function minimizers in finite time. However, in the case of a linear piece-wise gap function, each iteration of a subgradient method is capable of producing a linear cutting plane that can be added to the master problem and, when a sufficient set of cutting planes has been found, return the exact minimizer. By occasionally

solving the master problem between subgradient method steps, finite-time convergence can be guaranteed. Moreover, because subgradient methods do not need to solve the master problem at every iteration, it is possible that they may converge towards the function minimizer at a faster rate than traditional cutting plane algorithms. Subgradient methods also have the ability to query subgradients with respect to non-optimal FOP solutions for heuristic approximations and stochastic descent methods, which we explore in Section 6. With these ideas in mind, we implement solution methods that make use of two major methods from the literature; projected gradient descent (Boyd et al. 2003) and the Frank-Wolfe method (Frank and Wolfe 1956).

4.2.1. Projected gradient descent (PGD). To execute an iteration of projected gradient descent, given some step-size $t_k > 0$, we choose our next α with $\alpha^{(k)} \leftarrow \alpha^{(k-1)} - t_k(C(\hat{\mathbf{y}} - \mathbf{y}^{(k-1)}))$, and then project $\alpha^{(k)}$ onto its domain \mathcal{A} (Boyd et al. 2003). For a sufficiently small step size t_k , if $\alpha^{(k)}$ is not the minimizer of ξ_{ABS} , then $\alpha^{(k+1)}$ will yield a lower optimality gap. Further, there exist multiple choices of the sequence t_k such that the method will converge upon an optimal solution as k approaches infinity (Boyd et al. 2003).

REMARK 2. Once all facet-defining tangent planes that are tangent at the gap function minimizer are known, then a single run of the master problem will yield the exactly optimal solution. We can use this knowledge to create a descent method that will be guaranteed to terminate at an optimal solution rather than infinitely converge on it.

We formalize this idea as follows. Let $\xi_{\text{ABS}}(\alpha)$ be the absolute gap function generated by a polyhedral forward feasible region \mathcal{S} and an inverse input $\hat{\mathbf{y}}$. Let α^* be a minimizer of $\xi_{\text{ABS}}(\alpha)$. Let $\alpha^{(k)}$ be generated by a projected subgradient descent method that uses step-size sequence t_k , and let \mathcal{S}^k denote a set of FOP solutions $\mathbf{y}^{(0)} \dots \mathbf{y}^{(k)}$ found in the descent process. At every step k , a subtangent plane to $\xi_{\text{ABS}}(\alpha)$ at $\alpha^{(k)}$ is generated from $\mathbf{y}^{(k)} \in \mathcal{S}^k \supseteq \mathcal{S}^{k-1}$. If α^* is a unique minimizer of $\xi_{\text{ABS}}(\alpha)$, then it corresponds to a facet of $\text{conv}(\mathcal{B})$ that contains $\mathbf{C}\hat{\mathbf{y}} - \xi_{\text{ABS}}(\alpha^*)\mathbf{1}$ in its interior (proof that $\mathbf{C}\hat{\mathbf{y}} - \xi_{\text{ABS}}(\alpha^*)\mathbf{1}$ is contained on the boundary of $\text{conv}(\mathcal{B})$ follows from Theorem 1 (b) of Chan et al. (2014)). Similarly, each facet-defining tangent plane of $\xi_{\text{ABS}}(\alpha)$ corresponds to a vertex of $\text{conv}(\mathcal{B})$. Let B^k denote a set of points on the boundary of $\text{conv}(\mathcal{B})$ corresponding to \mathcal{S}^k , i.e. the set $\{\mathbf{C}\mathbf{y}^{(0)} \dots \mathbf{C}\mathbf{y}^{(k)}\}$. Finally, note that if α^* is not a unique minimizer, then the above is true for a lower dimensional face of $\text{conv}(\mathcal{B})$ rather than a facet.

PROPOSITION 3. *Suppose α^* is a unique minimizer of $\xi_{\text{ABS}}(\alpha)$. If the convex hull of B^k contains $\mathbf{C}\hat{\mathbf{y}} - \xi_{\text{ABS}}(\alpha^*)\mathbf{1}$ in the interior of one of its facets, then solving the master problem $\text{GIO}_{\text{ABS}}(\hat{\mathbf{y}}, \mathcal{S}^k)$ will yield α^* .*

We provide proof of this proposition in EC.1.1. As stated in the proof, if $\text{conv}(\mathcal{B})$ is a set of dimension $|\mathcal{K}|$, then there exists at least one set of only $|\mathcal{K}|$ elements of $\text{conv}(\mathcal{B})$ that need to be

discovered for this condition to be met. We henceforth refer to the case where solving the master problem yields the optimal solution as the *MP solve condition*.

DEFINITION 2 (MP SOLVE CONDITION). For a sequence $\boldsymbol{\alpha}^{(k)}$ generated by an inverse optimization solution method, the MP Solve Condition is achieved at an iteration k when solving $\text{GIO}_{\text{ABS}}(\hat{\mathbf{y}}, \mathcal{S}^k)$ yields $\boldsymbol{\alpha}^*$. As stated in Proposition 3, this occurs when $\text{conv}(B^k)$ contains $\mathbf{C}\hat{\mathbf{y}} - \xi_{\text{ABS}}(\boldsymbol{\alpha}^*)\mathbf{1}$ in the interior of one of its facets.

Our implementation of a terminating projected gradient descent solution algorithm is presented in Algorithm 1. Our algorithm iterates through steps of projected gradient descent, and then solves the master problem whenever a descent step neither decreases the gap function by the maximum expected amount nor returns a new FOP extreme point. This occurs when $\boldsymbol{\alpha}^{(k)\top}\mathbf{C}\hat{\mathbf{y}} - \boldsymbol{\alpha}^{(k)\top}\mathbf{C}\mathbf{y}^{(k)} > \boldsymbol{\alpha}^{(k-1)\top}\mathbf{C}\hat{\mathbf{y}} - \boldsymbol{\alpha}^{(k-1)\top}\mathbf{C}\mathbf{y}^{(k-1)} + (\boldsymbol{\alpha}^{(k)} - \boldsymbol{\alpha}^{(k-1)})\top(\mathbf{C}(\hat{\mathbf{y}} - \mathbf{y}^{(k-1)}))$ and $\mathcal{S}^k = \mathcal{S}^{k-1}$. One possible case when this occurs is when a sufficient number of facets of $\xi_{\text{ABS}}(\boldsymbol{\alpha})$ surrounding the minimizer have been found and the descent method is repeatedly travelling between them. In this case, the MP solve condition has been reached, and the final output of $\text{GIO}_{\text{ABS}}(\hat{\mathbf{y}}, \mathcal{S}^k)$, denoted $\boldsymbol{\alpha}^{\text{final}}$ will be the gap function minimizer $\boldsymbol{\alpha}^*$, which can be verified by solving the FOP with $\boldsymbol{\alpha}^{\text{final}}$. If the resulting gap function value is equal to the objective value of $\text{GIO}_{\text{ABS}}(\hat{\mathbf{y}}, \mathcal{S}^k)$, then $\boldsymbol{\alpha}^{\text{final}} = \boldsymbol{\alpha}^*$ and the algorithm terminates. If this FOP solve yields a different gap function value than the objective value returned by $\text{GIO}_{\text{ABS}}(\hat{\mathbf{y}}, \mathcal{S}^k)$, then the MP solve condition had not yet been reached. The termination criterion may have been reached by descent steps travelling between facets of $\xi_{\text{ABS}}(\boldsymbol{\alpha})$ that are not adjacent to the minimizer $\boldsymbol{\alpha}^*$, and thus the descent step size is too large. In this case, the step size is divided by two and iterations of projected gradient descent proceed until the termination criterion is reached again.

PROPOSITION 4. *Algorithm 1 (i) terminates in a finite number of iterations, and (ii) returns the gap function minimizer.*

Proof of Proposition 4 is provided in Appendix EC.1.2.

4.2.2. Accelerated projected gradient descent (PGD-A). We implement Polyak's Heavy Ball Method as part of Algorithm 1 by adding a momentum term with a coefficient $\beta \in (0, 1]$ to the step formulation before projecting onto the domain (Polyak 1964). We use the same termination method as in the projected gradient descent method. See Algorithm 4 in EC.7 for pseudocode of the algorithm structure with the addition of a momentum term, utilizing the same termination technique as projected gradient descent.

Algorithm 1: Gap-gradient projected gradient descent method.

```

input :  $C, \hat{\mathbf{y}}, \text{FOP}, t$ 
output:  $\alpha^{\text{best}}, \xi^{\text{final}}$ 
 $k = 0, \mathcal{S}^k \leftarrow \emptyset, \alpha^{(k)} \leftarrow \frac{1}{K} \mathbf{1};$ 
 $\mathbf{y}^{(k)} \leftarrow \text{FP}(\alpha^{(k)});$ 
 $\xi_{\text{ABS}} \leftarrow \alpha^{(k)\top} C \hat{\mathbf{y}} - \alpha^{(k)\top} C \mathbf{y}^{(k)};$ 
while  $\alpha^{(k)\top} C \hat{\mathbf{y}} > \alpha^{(k)\top} C \mathbf{y}^{(k)}$  do
   $k \leftarrow k + 1;$ 
   $\mathcal{S}^k \leftarrow \mathcal{S}^{k-1} \cup \mathbf{y}^{(k-1)};$ 
   $\alpha^{(k)} \leftarrow \alpha^{(k-1)} - t(C(\hat{\mathbf{y}} - \mathbf{y}^{(k-1)}));$ 
   $\alpha^{(k)} \leftarrow \text{proj}_{\Delta^{\mathcal{K}}}(\alpha^{(k)});$ 
   $\mathbf{y}^{(k)} \leftarrow \text{FOP}(\alpha^{(k)});$ 
  if  $\alpha^{(k)} = \alpha^{(k-1)}$  or  $\alpha^{(k)\top} C \hat{\mathbf{y}} - \alpha^{(k)\top} C \mathbf{y}^{(k)} > \xi_{\text{ABS}} + (\alpha^{(k)} - \alpha^{(k-1)})^\top (C(\hat{\mathbf{y}} - \mathbf{y}^{(k-1)}))$  and
     $\mathbf{y}^{(k)} \in \mathcal{S}^k$  then
       $\alpha^{\text{final}}, \xi^{\text{final}} \leftarrow \text{GIO}_{\text{ABS}}(\hat{\mathbf{y}}, \mathcal{S}^k);$ 
       $k \leftarrow k + 1;$ 
       $\mathbf{y}^{(k)} \leftarrow \text{FOP}(\alpha^{\text{final}});$ 
      if  $\alpha^{\text{final}\top} C \hat{\mathbf{y}} - \alpha^{\text{final}\top} C \mathbf{y}^{(k)} = \xi^{\text{final}}$  then
        | stop
      else
        |  $\alpha^{(k)} \leftarrow \alpha^{\text{final}};$ 
        |  $\mathcal{S}^k \leftarrow \mathcal{S}^{k-1} \cup \mathbf{y}^{(k-1)};$ 
        |  $t \leftarrow \frac{t}{2};$ 
      end
    else
      |  $\xi_{\text{ABS}} \leftarrow \alpha^{(k)\top} C \hat{\mathbf{y}} - \alpha^{(k)\top} C \mathbf{y}^{(k)};$ 
    end
  end
end

```

4.2.3. Frank-Wolfe method (FW). The Frank-Wolfe method of optimization over a convex bounded function entails querying the loss function gradient at a given point, finding the minimizer of said gradient in the function domain, and moving in the direction towards said point with a step size that decreases at a rate of $O(\frac{1}{k})$. In our case, the domain of the function we are minimizing (\mathcal{A}) is a unit simplex, so the task of finding the gradient minimizer is trivial; we find the smallest component i of the gradient, and the minimizer is the vector with 1 at component i and 0 for all others. For a Lipschitz-continuous convex function (e.g., the absolute gap function, ξ_{ABS}), the algorithm converges on an optimal solution at a rate of $O(\frac{1}{k})$ (Frank and Wolfe 1956).

See Algorithm 5 in EC.7 for our implementation of the Frank-Wolfe method in the context of generalized inverse optimization, using the same termination method as projected gradient descent.

REMARK 3. We note that it is actually possible to converge on the optimal solution using the Frank-Wolfe method without necessarily being able to query the gradient accurately, so long as one can find the point in the gap space that minimizes said gradient. For the case where the loss function is absolute sub-optimality and \mathcal{A} is the unit simplex, we only need to consider $|\mathcal{K}|$ such points in our domain, so it may be possible to not solve the forward problem to completion, as long as we do enough work to be certain which of these points would be the gradient minimizer (i.e., the optimal solution will produce a gradient with a specific component being the smallest). As soon as we know this, we can abort solving the forward problem and take the next Frank-Wolfe step. Since solving the MIP forward problem is generally the most computationally complex step of all algorithms discussed so far, this has the potential to significantly improve time-per-iteration in the Frank-Wolfe algorithm (and thus potentially in overall time). However, if our method of executing early cutoffs is not able to accurately query the gap function value and yield tangent planes, we will not be able to *only* conduct partial FOP solves and then terminate the algorithm with an MP solve condition. However, one may choose to run several partial solve iterations before changing the approach and using fewer full solve iterations in a close neighborhood of the solution before terminating. Note that the gap function tangent planes generated when far from the solution are not necessarily useful for terminating the master problem, and only those planes tangent to facets that include a function minimizer need to be known.

We provide a formal method for operationalizing this idea in EC.4, but we leave the practical implementation of this approach for future work.

5. Experimental Evaluation of Solution Methods

In this section, we evaluate our proposed methods and compare them to an existing method using a set of multi-objective inverse mixed integer optimization problems derived from FOPs obtained from the MIPLIB 2017 mixed integer programming library (Gleixner et al. 2021).

5.1. Experimental Setup

We implement and compare our three proposed solution methods: 1) projected gradient descent (PGD), 2) accelerated projected gradient descent (PGD-A), and 3) Frank-Wolfe method (FW). We compare our approaches with the only applicable solution method from the literature: the Moghaddass-Terekhov cutting plane method (CP) (Moghaddass and Terekhov 2020). For PGD and PGD-A, the initial step size is chosen so that the Euclidean norm of the first descent step is 0.1, i.e. $\|\alpha^{(1)} - \alpha^{(0)}\|_2 = 0.1$. For PGD-A, we use a momentum coefficient of 0.5. We note that our approach produces a conservative estimate for the performance of these methods because a

more rigorous search for optimal step sizes and momentum coefficients may substantially improve solution times.

The list of selected MIPLIB instances (i.e., FOPs) is included in EC.6.1. These nine instances were chosen because (1) they were flagged as “benchmark-suitable” and rated as “easy” solution difficulty, allowing for relatively tractable run times for the inverse solution algorithms, (2) they contained at least 128 continuous variables which can serve as reasonable sub-objectives, in addition to containing integer or binary variables, (3) they were neither infeasible nor unbounded for any sampled objective weights α in our computational trials, and (4) they span a variety FOP structures that are suited for different application settings.

To adapt each of the nine FOPs into a multi-objective generalized inverse optimization problem, we conduct the following process. For each value of k in the sequence [4, 8, 16, 32, 64, 128]:

1. We randomly sample k continuous variables from the FOP formulation to be the individual sub-objectives. Each sub-objective function in our multi-objective formulation is the value of one of these sampled variables. Thus each row in the matrix \mathbf{C} contains all entries equalling 0 except for one sampled variable, which has coefficient 1. We execute this sampling process 3 times per FOP.
2. For each sampled matrix \mathbf{C} , we sample 3 different coefficient vectors α from the unit simplex in k dimensions.
3. For each sampled combination of \mathbf{C} and α , we solve the FOP with the objective function $\alpha^T \mathbf{C} \mathbf{y}$ to obtain our inverse input solution $\hat{\mathbf{y}}$. In total, this gives us 9 inverse inputs per FOP formulation (per k).
4. We used each of the four inverse solution methods to solve the inverse optimization problem for each of the nine input solutions. We use the absolute sub-optimality loss function and the unit simplex for the set of allowable objectives. For each solve, we record the total run time and the total number of iterations.

All computational experiments were executed on an HP EliteDesk 800 G4 TWR with an Intel(R) Core(TM) i5-8500 CPU running at 3.00GHz with 6 Cores and 6 Logical Processors and 16.0 GB of RAM. All code was written and executed in Python version 3.7.3 and all FOPs were solved using Gurobi version 9.0.2. A maximum running time of 360 seconds was used in each trial before cutting off the solution algorithms.

5.2. Results

Figure 2 displays the median solution times of each novel algorithm in comparison to CP. PGD, PGD-A, and FW improved upon CP in 27, 30, and 26 of the 54 instances, respectively. For those instances where our methods did not improve upon CP, the performance was similar. Figure 3

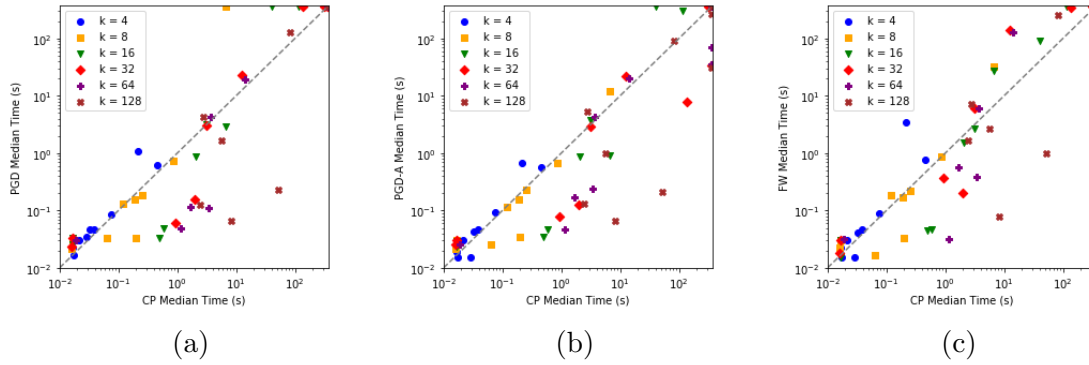


Figure 2 A comparison of median solution times for each value of k (marker type): (a) PGD vs. CP, (b) PGD-A vs. CP, and (c) FW vs. CP. For each marker type (value of k), there are nine markers (one for each FOP instance) that denote the median solution time across all samples for that FOP instance.

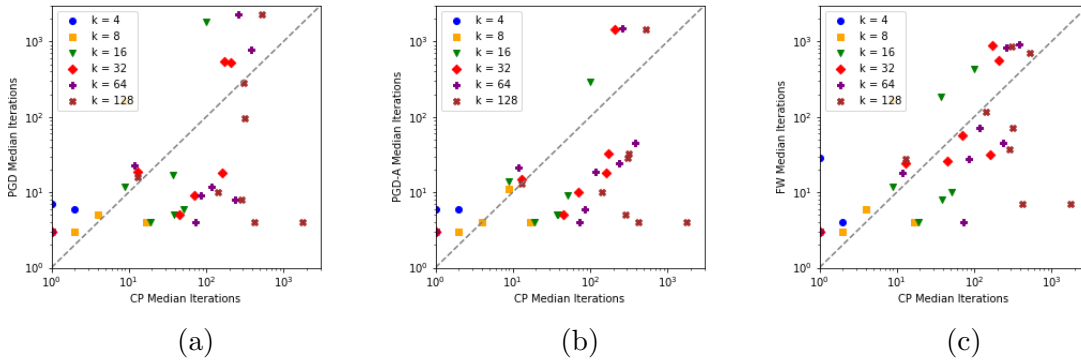


Figure 3 A comparison of the median number of iterations for each value of k (marker type): (a) PGD vs. CP, (b) PGD-A vs. CP, and (c) FW vs. CP.

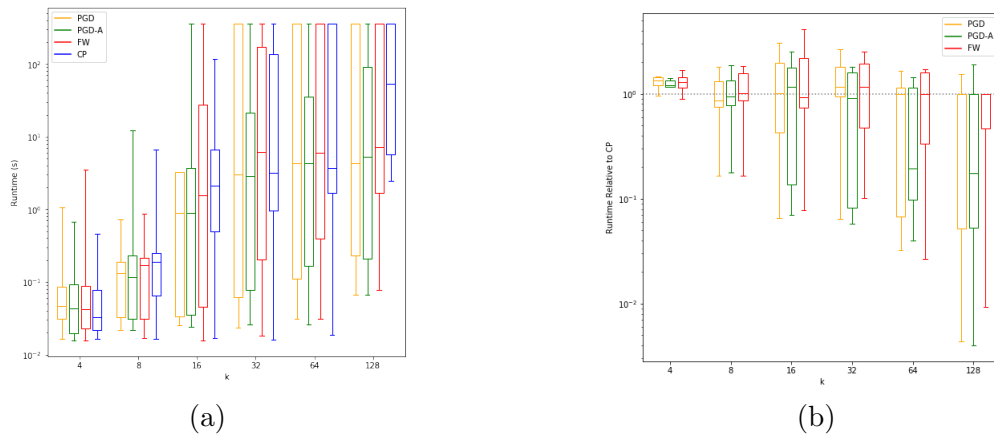


Figure 4 Boxplots for each value of k of: (a) the median runtimes across FOP instances, and (b) the ratio of median runtimes compared to CP median runtime for the 3 gap-gradient methods.

displays the median iteration count of each novel algorithm in comparison to CP. By design of the termination criterion, our gap-gradient methods take a minimum of 3 iterations before terminating, and for many instances where $k = 4$, the initialized value of $\alpha^{(0)} = \frac{1}{k}\mathbf{1}$ is a loss function minimizer, and thus can be completed in one iteration by the CP method.

Figure 4 displays boxplots of the median solution time for each of the four methods and the improvement in median solution time over CP. The median solution time (\pm standard deviation) as a function of k for CP was 0.03s (± 0.14), 0.19s (± 2.01), 2.10s (± 37.0), 3.17s (± 137.2), 3.75s (± 168.5), 53.1s (± 160.0). The median solution time (\pm standard deviation) for our best performing implementation (PGD-A) was 0.04s (± 0.24), 0.12s (± 3.82), 0.88s (± 137.5), 2.91s (± 111.1), 4.29s (± 110.3), 5.29s (± 128.1). The median improvement in median solution time as a function of k was -0.01s (-33.3%), 0.07s (36.8%), 1.22s (58.1%), 0.26s (8.2%), -0.54s (-14.4%), and 47.81s (90.0%).

6. Application to Political Gerrymandering

In this section, we present the FOP used for political districting (Section 6.1), present custom solution approaches based on graph coarsening and ensemble methods (Section 6.2), and then evaluate our solution approaches using randomly generated problem instances (Section 6.3). In the following section (Section 7), we present a case study using real data from the State of Iowa.

6.1. Forward optimization problem (FOP)

We use the political districting model from Swamy et al. (2022) as our FOP. The model is a mixed-integer linear program that determines the political districting for a given state. Let $G = \{V, E\}$ be a graph where each vertex $v \in V$ represents a census block or some larger tract of land within the state and edges $e \in E$ represent the adjacency of such areas. Each vertex v is associated with a population $p_v \in V$, the number of democratic (republican) voters $p_v^D(p_v^R), v \in V$, and an area (in square feet) $a_v, v \in V$. We let $d_{i,j}, i, j \in V$ represent the Euclidean distance between vertex i and j (not necessarily adjacent).

Let the decision variables x_{ij} be a binary indicator of whether the vertex $i \in V$ is the center of a district that contains the vertex $j \in V$. The decision variable f_{ijv} indicates a network flow between vertices j and $v \in V$ where they both have district center i , which is used to maintain contiguity of modeled districts. The binary decision variable z_i^D indicates if the district with center i is won by the Democratic party, and v_{ij}^D indicates whether or not j is in a district with center i which is won by the Democratic party. Finally, the decision variable w_i indicates the number of wasted Democratic votes minus the number of wasted Republican votes in the election in the district with center i .

Intuitively, the model solution determines a partition of the graph G into L disjoint connected subgraphs, which denote the legislative districts. We provide the full FOP formulation in

Appendix EC.5. We define the objective of the FOP as a weighted sum of three components: a measure of population imbalance, a measure of compactness, and a measure of efficiency gap.

6.1.1. Population imbalance (ρ). We let ρ represent the population imbalance measured as the largest relative deviation from the average district population exhibited by any district.

$$\rho = \frac{\max_{i \in V} \left| \sum_{j \in V} p_i x_{ij} - \frac{\sum_{j \in V} p_j}{L} \right|}{\frac{\sum_{j \in V} p_j}{L}}$$

For example, in a state of population 1000, ten districts of population 100 would yield $\rho = 0$, while nine districts with population 101 and one of population 91 would yield $\rho = \frac{|91-100|}{100} = 0.09$. Unlike Swamy et al. (2022), we include population imbalance in the objective rather than a constraint because the current legal text and judicial practice indicates that district populations should be *as close to equal as possible*, clearly indicating it as an objective to be minimized.

6.1.2. Compactness (σ_A). We let σ_A represent the compactness of a districting. Compactness is formulated as a measure of the p-median distance weighted by the area of each tract of land, divided by the area-weighted 1-median distance of the entire state (denoted by M). Using our notation, this can be written as:

$$\sigma_A = \frac{\sum_{i,j \in V} d_{ij} a_j x_{ij}}{M}$$

6.1.3. Efficiency gap (ϕ_{EG}). We let ϕ_{EG} denote the efficiency gap, measured as defined by Stephanopoulos and McGhee (2015) using a set of constraints formulated by Swamy et al. (2022). The measurement of the efficiency gap is motivated by the construction and counting of *wasted votes*, which contain both votes cast for a losing candidate and votes cast for a winning candidate beyond the necessary majority. The relative disparity in wasted votes distributed across two major parties as the result of district-based elections is measured as the efficiency gap, which can be calculated as:

$$\phi_{EG} = \frac{\left| \sum_{i \in V} w_i \right|}{\sum_{i \in V} p_i^D + p_i^R}$$

The construction of this metric directly targets districting tactics known as *cracking* and *packing*, which are alleged to be a major strategy of partisan gerrymandering.

Since this problem is very computationally taxing to solve, Swamy et al. (2022) propose a graph coarsening approach to reduce the size of the problem formulation.

6.2. Graph coarsening

In this section, we present custom solution approaches for graph based inverse mixed integer optimization problems. Our approach uses a combination of graph coarsening with ideas from machine learning and data-driven inverse optimization. Although these methods were inspired by our application of political districting, they can be applied to any inverse optimization problem where the FOP can be represented as a graph-based problem.

6.2.1. Maximal matching. Basic graph coarsening is achieved by producing a random maximal matching of the edges of the graph and contracting all edges in the produced matching into vertices. A random maximal matching is produced by iterating through a random ordering of the edges, and selecting an edge to be contracted if both of its endpoints are not adjacent to any edges that have already been selected for contraction. All population and area data at the endpoints of a contracted edge is summed together to produce the data for the newly formed vertex, and the distances associated with the edges of newly formed vertices are calculated from landmass centroids derived from area-weighted averages of the two contracted endpoints. This process can be iteratively repeated as many times as desired to shrink the graph to a needed size. Overall, this process produces a smaller graph with the same underlying spatial structure but at a lower data resolution. This allows for a problem that is less computationally taxing, at a tradeoff of reduced accuracy of the final solution due to lower data resolution.

Swamy et al. (2022) suggest that coarsening methods that choosing matchings that prioritize merging vertices with a low combined population preserve solutions with lower population imbalances, and lower objectives values for many subobjectives, with the same improvement on computational efficiency as random maximal matchings. As such, their method is deterministic, producing an ordering of edges by directly ranking the combined populations.

We propose a variation that still involves random choices of edges (which we exploit in the next section), while gaining the advantage of coarsenings that preserve better solutions. As such, our method creates an ordering of edges by sampling an exponential random variable for each edge with a mean of the combined population divided by twice the mean vertex population, and ordering by the edges by the values of the random samples. We note that if all edges have identical combined populations, then this method produces the same distribution of outputs as a random maximal matching method.

6.2.2. Ensemble-based coarsening. We leverage the idea of *ensembles* from machine learning to produce and exploit multiple coarsenings of the same graph (Breiman 1996). Since both the basic maximal matching and our proposed variation are non-deterministic, multiple (different) coarsenings of the same graph can be produced with the same method. While each coarsening loses some resolution, elements lost in one coarsening may be preserved in another. An ensemble-based approach may allow for the risks of coarsening to be reduced in the aggregate, while potentially preserving the computational savings of coarsening. Let $FOP_1, FOP_2 \dots FOP_n$ denote the forward optimization problems generated for an ensemble of n different coarsenings of a political districting FOP, and let $\mathcal{S}_1, \mathcal{S}_2 \dots \mathcal{S}_n$ denote their respective feasible regions. We present two options for how an ensemble of coarsenings can be used to produce heuristic solutions to the inverse problem:

1. **Solve each instance independently.** In this approach, we solve an inverse model independently on each coarsened graph, generating the inverse solution α_i^* from each individual inverse formulation $\text{GIO}_{\text{ABS}}(\hat{\mathbf{y}}, \mathcal{S}_i)$. The average of the outputs, $\frac{1}{n} \sum_{i \in 1 \dots n} \alpha_i^*$, can then be used as an approximation of the true α^* . Alternatively, the set of inverse solutions can be analyzed as a distribution. For example, the convex hull of the set of outputs can be interpreted as a polytope of potential inverse solutions.
 2. **Solve a multi-point formulation.** In this approach, we solve a single multi-point inverse optimization formulation produced by creating a master problem with constraints that are derived from multiple coarsened graphs at once. A single slack variable describes the optimality gap across all constraints, thus minimizing the maximum optimality gap across all coarsenings.
- For the remainder of this section, we focus on the second approach, which can be formalized as the following optimization problem:

$$\begin{aligned}
& \underset{\alpha, \xi_{\text{ENS}}}{\text{minimize}} && \xi_{\text{ENS}} && (\text{MultiGIO}_{\text{ABS}}\text{MinMax}) \\
& \text{subject to} && \alpha^\top \mathbf{C} \mathbf{y}^0 \leq \alpha^\top \mathbf{C} \mathbf{y} + \xi_{\text{ENS}}, \quad \forall \mathbf{y} \in \mathcal{S}_1, \mathcal{S}_2, \dots, \mathcal{S}_n, \\
& && \|\alpha\|_1 = 1, \\
& && \alpha \geq \mathbf{0}, \quad \xi_{\text{ENS}} \geq 0.
\end{aligned}$$

For $\text{MultiGIO}_{\text{ABS}}\text{MinMax}$, we can show that as the size of the ensemble approaches infinity, the likelihood of our method finding the same solution as the full resolution graph approaches 1.

THEOREM 1. *Given an ensemble of n independently sampled coarsenings of G down to $v \geq L$ vertices, such that any coarsened graph with v vertices has a non-zero probability of being sampled, as $n \rightarrow \infty$, the probability of $\text{MultiGIO}_{\text{ABS}}\text{MinMax}$ yielding $\alpha^* =$ approaches 1.*

Proof of Theorem 1 is provided in Appendix EC.1.3. In the context of implementing gap-gradient methods for the multipoint inverse formulation, the coarsening that returns the highest optimality gap at the hypothesis $\alpha^{(k)}$ determines the next step in the descent process.

PROPOSITION 5. *Let $FOP_1, FOP_2 \dots FOP_n$ denote the forward optimization problems generated for an ensemble of n different coarsenings of a political districting FOP, and let $\xi_{\text{ENS}}(\alpha)$ denote the gap function corresponding to the multipoint inverse formulation $\text{MultiGIO}_{\text{ABS}}\text{MinMax}$ generated by this ensemble of coarsenings. Let $\alpha^{(k)}$ be the hypothesis cost vector at iteration k of a solution method for $\text{MultiGIO}_{\text{ABS}}\text{MinMax}$, and let $\mathbf{y}_i^{(k)}$ denote the optimal solution of $FOP_i(\alpha^{(k)})$. At any $\alpha^{(k)}$, the subgradient of $\xi_{\text{ENS}}(\alpha)$ is equal to $\mathbf{C}(\hat{\mathbf{y}} - \arg \min_{\mathbf{y} \in \mathbf{y}_1^{(k)} \dots \mathbf{y}_n^{(k)}} (\alpha^{(k)\top} \mathbf{C} \mathbf{y}))$.*

Proof of Proposition 5 is provided in Appendix EC.1.4.

Since the loss function $\xi_{\text{ENS}}(\alpha)$ satisfies all the properties listed in Remark 1, the gap-gradient methods described in Section 4.2 may be used to find solutions to $\text{MultiGIO}_{\text{ABS}}\text{MinMax}$.

6.2.3. Stochastic descent with coarsened ensembles. In this section, we demonstrate how stochastic gradient descent can be used with coarsening to solve generalized inverse optimization problems with graph-based FOPs. Instead of generating an ensemble of coarsenings to create a lower approximation ξ_{ENS} of ξ_{ABS} , and then deterministically minimizing the approximation, one can instead use ensembles of coarsenings to produce estimators of subgradients of ξ_{ABS} in the application of a stochastic gap-gradient method to an inverse model formulated for the full sized graph. Similar to the multipoint formulation method, our gradient approximation is calculated as $\nabla \xi_{\text{ABS}}(\boldsymbol{\alpha}^{(k)}) \approx \mathbf{C}(\hat{\mathbf{y}} - \arg \min_{\mathbf{y} \in \mathbf{y}_1^{(k)} \dots \mathbf{y}_n^{(k)}} (\boldsymbol{\alpha}^{(k)\top} \mathbf{C}\mathbf{y}))$. However, in this application, an ensemble of coarsenings $\text{FOP}_1^{(k)}, \text{FOP}_2^{(k)} \dots \text{FOP}_n^{(k)}$ is independently randomly sampled during each iteration k of the subgradient method. Here the use of coarsenings and ensembles is analogous to the process of mini-batching in stochastic gradient descent for training neural networks, where the true loss function gradient is estimated by calculating the loss function with respect to a randomly sampled subset of the the full set of available samples (Schmidt 2019). In neural networks, the samples come from the set of training observations; in the inverse graph partitioning case, ‘samples’ come from the set of possible partitions \mathcal{S} , and each coarsened graph contains contains a subset of such samples.

It is not obvious that solving the FOP on coarsened graphs or ensembles thereof yields an unbiased estimator of $\nabla \xi_{\text{ABS}}$. However, Theorem 1 does show that approximating the gradient of ξ_{ABS} with $\mathbf{C}(\hat{\mathbf{y}} - \arg \min_{\mathbf{y} \in \mathbf{y}_1^{(k)} \dots \mathbf{y}_n^{(k)}} (\boldsymbol{\alpha}^{(k)\top} \mathbf{C}\mathbf{y}))$ constitutes a *consistent and asymptotically unbiased estimator* of $\nabla \xi_{\text{ABS}}$, as defined by Chen and Luss (2019). Under the conditions of a convex but not strongly convex gap function (such as absolute sub-optimality), when using a subgradient estimation method where expected estimation error is inversely proportional to \sqrt{k} , stochastic projected gradient descent observes a convergence rate of $O(\frac{1}{\sqrt{k}})$ towards the gap function minimum value. To obtain this bound for the coarsening application, the subgradient estimation must involve progressively larger ensembles with each iteration. Without progressively increasing the ensemble size, we can expect our method to converge to the neighborhood of the minimizer, but is not guaranteed to find the exact minimizer.

Algorithm 9 presents the structure of an implementation of stochastic subgradient estimation within a projected gradient descent approach to loss function minimization, where n_k indicates a rule for selecting a coarsening ensemble size at a given iteration k , and K denotes a maximum number of iterations. At the end of K iterations, a weighted averaging of the values of $\boldsymbol{\alpha}^{(k)}$ is returned. We note that the termination criterion utilized in Section 4.2 are much less likely to be triggered at any given iteration. As such, in our evaluation of stochastic subgradient methods, we examine how closely the descent methods approach the true loss function minimum and minimizer, rather than comparing the time until termination yielding an exact minimizer, as in the previous computational evaluations.

6.2.4. Boosted ensembles of coarsenings. To accentuate the diversity of the ensemble of coarsened graphs, we implement a method of sequential coarsening inspired by boosting ensemble methods from machine learning (Schapire 1999). In an unboosted coarsening implementation, the random maximal matching of a graph is determined by creating a uniformly randomly ordered list of the edges, proceeding through the list in order, and contracting each edge if and only if both endpoints are not adjacent to an edge that has already been contracted. The random shuffling that determines each coarsening is independent for each element of the ensemble. In a *boosted implementation*, the randomly ordered shuffling of the edges is done in a weighted fashion such that an edge with a higher weight is more likely to be later in the ordering. In coarsening the first element of the ensemble, either the initial edge weights are uniform, or weighted by population as detailed in Section 6.2.1. If an edge $e \in E$ is contracted when creating the i^{th} element of the ensemble, then for the $(i + 1)^{\text{th}}$ element, the weight of edge e is multiplied by a factor $\eta > 1$, and its weight is multiplied by $\frac{1}{\eta}$ otherwise. This ensures that every ensemble member is less likely to have certain edges contracted that were frequently contracted in previous coarsenings, discouraging highly correlated coarsenings in the ensemble. This process is detailed in ECEC.7 (Algorithm 8). In the case of ensembles of graphs coarsened multiple times over, this process can be repeated at each tier of coarsening in a tiered tree-like fashion until the desired depth of coarsening is reached.

6.3. Computational Experiments

In this section, we evaluate our solution approaches using randomly generated problem instances representative of political districting.

6.3.1. Experimental setup. To evaluate our models, we use 8 simulated graphs/states of size $|G| = 20$. See EC.6.2 for details on how we simulate a state. For each graph/state, we create 5 uniformly randomly sampled multi-objectives weightings, and solve the corresponding FOP to create 5 inverse inputs for each simulated state. In total, we have 40 simulated IO instances. For each instance, we perturb the value of each subobjective by adding a random value in the range $[0.0375, 0.0625]$; this allows us to find an interior point that is likely to have a unique gap function minimizer. We solve each instance to optimality without any coarsening as a benchmark.

We conduct three experiments. First, we evaluate the impact of coarsening on the accuracy of inverse optimization solutions. We evaluate two coarsening methods: contracting edges selected from a random maximal matching of vertices and contracting edges selected from a population-weighted maximal matching. For each method, we conduct both one and two rounds of coarsening for each of the 40 problem instances. We then solve an IO problem for each instance using the PGD-A method to obtain a heuristic solution α^h .

Second, we evaluate the efficacy of the multi-point ensemble formulation as a heuristic for minimizing the gap function. We generate coarsened graphs with one round of random maximal matching, and we create ensembles of size 1, 4, 16, and 64, using both the independently random coarsening and the boosted coarsening techniques described in Section 6.2.4 with learning rate $\eta = 1.5$. For each ensemble, we apply the multi-point inverse formulation $\text{MultiGIO}_{\text{abs}}\text{MinMax}$ on the ensemble to achieve the heuristic solution $\boldsymbol{\alpha}^h$.

Third, we evaluate the performance of stochastic descent methods on estimating the gap function minimizer. We apply stochastic descent methods with unboosted ensembles of sizes 16 and 64, and an increasing ensemble rule $n = k$. For the descent methods, a step size is automatically chosen such that the first step has length 0.1, with following step sizes decreasing at a rate of $\frac{1}{\sqrt{k}}$, and a momentum coefficient of 0.1. We run each descent algorithm for a total of 12 iterations and return a heuristic solution $\boldsymbol{\alpha}^h$ at iterations 0, 4, 8, and 12.

For each experiment, we record the total solution time, the gap function value of the returned output cost vector minus the true gap function minimum value (i.e., $\xi_{\text{ABS}}(\boldsymbol{\alpha}^h) - \xi_{\text{ABS}}(\boldsymbol{\alpha}^*)$), and the Euclidean distance between the returned cost vector and the optimal cost vector (i.e., $\|\boldsymbol{\alpha}^h - \boldsymbol{\alpha}^*\|_2$).

6.3.2. Experimental results. Figure 5a displays the gap function value of the returned output cost vector minus the true gap function minimum value (i.e., $\xi_{\text{ABS}}(\boldsymbol{\alpha}^h) - \xi_{\text{ABS}}(\boldsymbol{\alpha}^*)$). For coarsening by random maximal matching, the median (standard deviation) difference was 0.21 (0.14) and 0.39 (0.16) for 1 and 2 rounds of coarsening, respectively. For coarsening by population-weighted matching, the median (standard deviation) difference was 0.37 (0.26) and 0.46 (0.27) for 1 and 2 rounds of coarsening, respectively. Figure 5b displays the Euclidean distance between the returned cost vector and the optimal cost vector (i.e., $\|\boldsymbol{\alpha}^h - \boldsymbol{\alpha}^*\|_2$). For coarsening by random maximal matching, median (standard deviation) distance was 0.43 (0.31) and 0.75 (0.33) for 1 and 2 rounds of coarsening, respectively. For coarsening by population-weighted matching, median (standard deviation) distance was 0.57 (0.33) and 0.60 (0.43) for 1 and 2 rounds of coarsening, respectively. Overall, random maximal matching produced solutions that were closer to the optimal solution as compared to population-weighted matching.

Figure 6a displays $\xi_{\text{ABS}}(\boldsymbol{\alpha}^h) - \xi_{\text{ABS}}(\boldsymbol{\alpha}^*)$. For unboosted ensembles, the median (standard deviation) difference was 0.0071 (0.075), 0.0045 (0.014), 0.0050 (0.0079), and 0.0045 (0.0046), for ensembles of size 1, 4, 16, and 64, respectively. For boosted ensembles, the median (standard deviation) difference was 0.021 (0.092), 0.016 (0.048), 0.0051 (0.0053), and 0.0036 (0.0043), for ensembles of size 1, 4, 16, and 64, respectively. Overall, an unboosted ensemble of size 64 was able to reduce the median and standard deviation of $\xi_{\text{ABS}}(\boldsymbol{\alpha}^h) - \xi_{\text{ABS}}(\boldsymbol{\alpha}^*)$ by 0.0026 (37%) and 0.704 (93%) over an ensemble of size 1, respectively. Figure 6b displays $\|\boldsymbol{\alpha}^h - \boldsymbol{\alpha}^*\|_2$. For unboosted ensembles, the

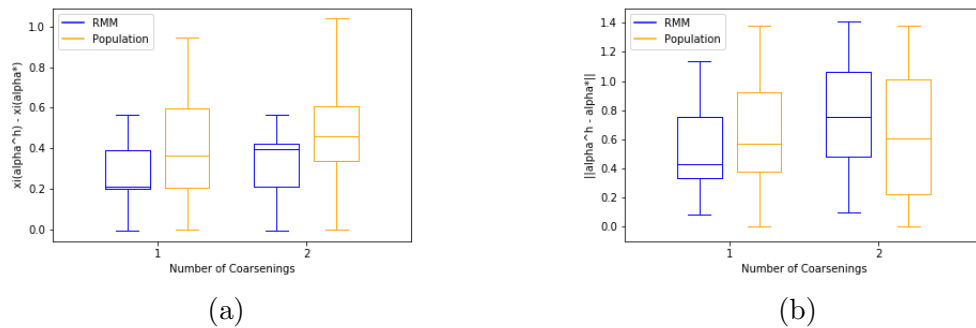


Figure 5 A comparison of (a) the difference between retrieved and true optimality gap, and (b) the distance from the original objective for different numbers of coarsenings.

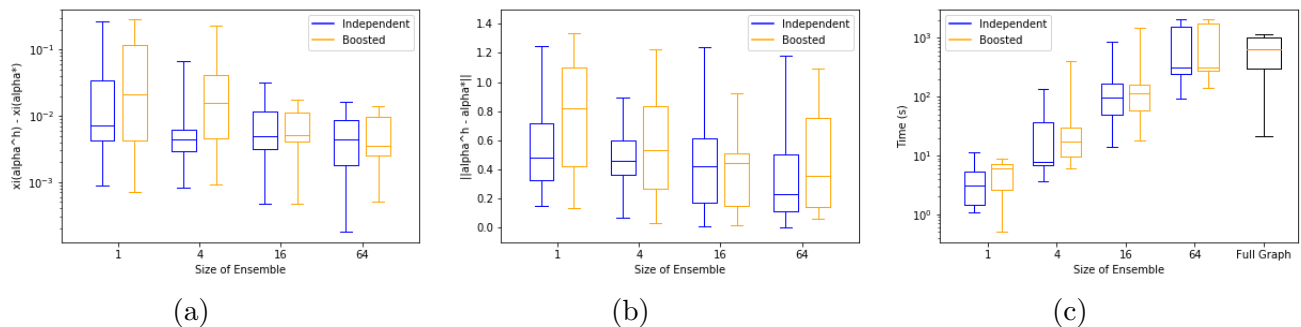


Figure 6 A comparison of (a) the difference between retrieved and true optimality gap, (b) the distance from the original objective, an (c) the solution time for various ensemble sizes.

median (standard deviation) distance was 0.48 (0.28), 0.46 (0.20), 0.42 (0.31), and 0.23(0.30), for ensembles of size 1, 4, 16, and 64, respectively. For boosted ensembles, the median (standard deviation) distance was 0.82 (0.36), 0.53 (0.36), 0.45 (0.26), and 0.35 (0.33), for ensembles of size 1, 4, 16, and 64, respectively. Overall, an unboosted ensemble of size 64 was able to reduce the median distance by 0.25 (52%) over an ensemble of size 1. Figure 6c displays the solution time; an unboosted ensemble of size 64 was able to reduce the median and standard deviation of the solution time of the full graph by 341s(52%) and -396s (-10%), respectively.

Figure 7a displays $\xi_{\text{ABS}}(\alpha^h) - \xi_{\text{ABS}}(\alpha^*)$. For stochastic descent, the median (standard deviation) difference after 12 iterations was 0.0031 (0.0047), 0.0037 (0.0036), and 0.0056 (0.0083), for ensembles of size 16, 64, and increasing size, respectively. Figure 7b displays $\|\alpha^h - \alpha^*\|_2$. The median (standard deviation) difference after 12 iterations was 0.37 (0.18), 0.40 (0.19), and 0.38 (0.31), for ensembles of size 16, 64, and increasing size, respectively. Figure 7c displays the solution time; 12 iterations of stochastic descent with an ensemble size of 64 was able to reduce the median and standard deviation solution time of the full graph by 55s (11%) and 211s (71%), respectively.

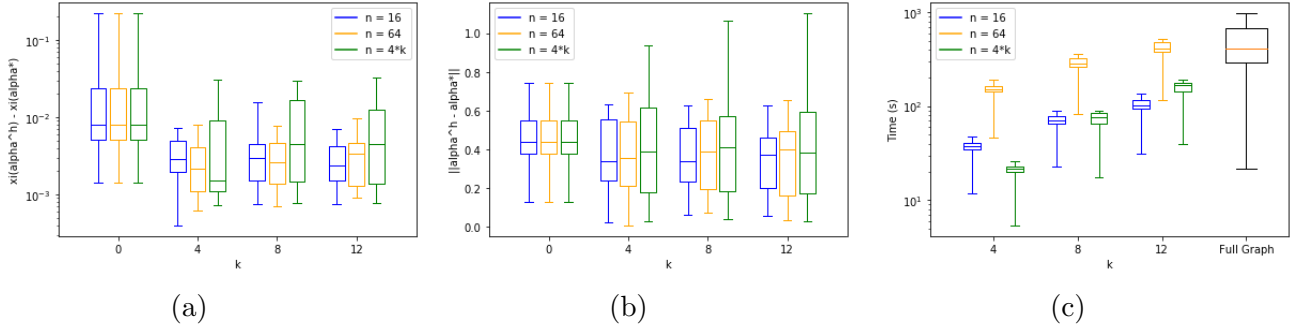


Figure 7 A comparison of (a) the difference between retrieved and true optimality gap, (b) the distance from the original objective, (c) the running time.

Overall, these results suggest that a multi-point formulation with an ensemble of 64 unboosted graphs coarsened by random maximal matching performs best in providing accurate approximations, while still providing decreased solution times.

7. Case Study: the State of Iowa

To demonstrate the application of inverse optimization to political gerrymandering, we applied our methods to the current congressional districts for the state of Iowa.

7.1. Context

Iowa’s 2022 congressional districts were designed by an independent districting commission. The first set of districts submitted by the commission were rejected by the state legislature. A second set of districts returned by the commission was subsequently approved by the state legislature.

Congressional districting in Iowa is unique in that the state constitution requires that counties are not split by district borders. The Iowa constitution also provides specific guidelines on how district compactness is to be measured (Iowa Code section 42.2). Two possible metrics are defined; *length-width compactness*, which is calculated as the absolute value of the difference in a district’s east-west distance and its north-south distance, and *perimeter compactness*, which is calculated as the perimeter of a district. We modify our FOP to measure compactness as the sum of the perimeter distance of each district, divided by the state perimeter times the number of districts (to scale the metric to the same range as the other sub-objectives). Perimeter compactness was chosen over length-width compactness as there exist numerous examples of possible districts with near-0 length-width compactness that by most common-sense approaches may be considered very non-compact, and while perimeter compactness may be susceptible to ‘coastline paradoxes’ that can make perimeter measurements not correspond to the broader shape of a district, the majority of Iowa’s counties are rectilinear in their boundaries, making this issue mostly irrelevant.

Let σ_P denote the perimeter compactness, let q_{ij} be binary variable indicating if adjacent vertices i and j are in different districts, let b_{ij} represent the length of the border shared by counties i and

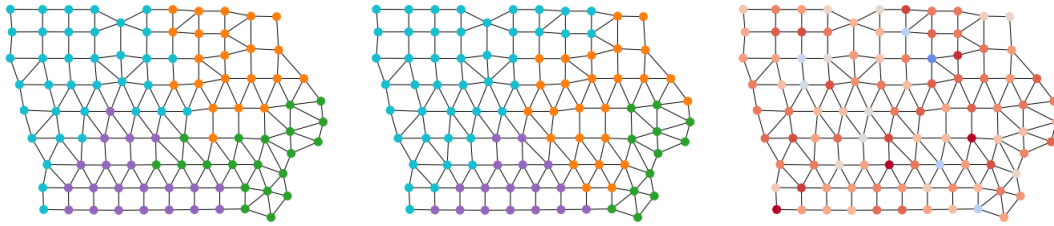


Figure 8 The full-sized graph of Iowa Counties, with color and shape denoting (a) the enacted 2022 districts, (b) the initially proposed and rejected 2022 districts, and (c) by relative partisan slant of the population in 2020 statewide elections

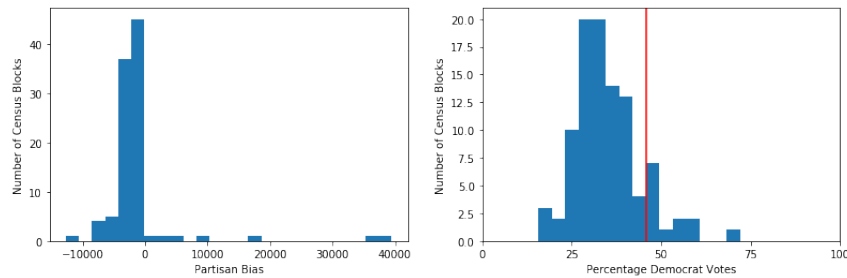


Figure 9 Distribution of (a) number of Democrat votes minus Republican votes and (b) percentage of votes towards Democrats by county

j , and let M_p represent the perimeter distance of the state of Iowa. We represent the metric using the following constraints:

$$q_{ij} \geq x_{ki} - x_{kj}, \quad \forall i, j, k \in V, b_{ij} \neq 0, \quad (2t)$$

$$\sigma_P = \frac{(\sum_{i,j \in V} q_{ij} b_{ij}) + M_p}{LM_p}, \quad (2u)$$

$$q_{ij} \in \{0, 1\}, \quad \forall i, j \in V, b_{ij} \neq 0. \quad (2v)$$

7.2. Data

State data for Iowa districts and electoral data were obtained from the Metric Geometry and Gerrymandering Group and the ALARM Project (McCartan et al. 2022). The full-sized graph of Iowa comprises 99 counties, partitioned into 4 districts. Figure 8 shows the full-sized graph of the state. The first subfigure displays the current assignment of counties into 4 districts (4 colours), the second subfigure displays the initially proposed 4 districts, and the final subfigure displays the relative partisan slant of voters in 2020 statewide elections, with blue indicating more Democrats and red indicating more Republicans.

Figure 9 (a) and (b) display the distribution of the difference between Democrat and Republican votes across the Iowa counties in the 2020 presidential election (the positive side of the x-axis represents more Democrat votes) by absolute difference and per capita percentages, respectively.

Metric	Rejected Value	Accepted Value
Perimeter Compactness (σ_P)	0.5773	0.6116
Population Imbalance (ρ)	$7.8674 * 10^{-5}$	$6.6137 * 10^{-5}$
Efficiency Gap (ϕ_{EG})	0.0882	0.4163

Table 1 Iowa Case Study Inverse Inputs

District	Population	Population Deviation	Perimeter	% Democrat
1	797,655	0.008%	503.03	54.6%
2	797,556	0.005%	786.27	44.9%
3	797,584	0.001%	515.54	49.9%
4	797,574	0.002%	967.18	34.9%

Table 2 Iowa Rejected Individual District Metrics

District	Population	Population Deviation	Perimeter	% Democrat
1	797,584	0.001%	696.48	49.0%
2	797,589	0.00037%	624.17	48.1%
3	797,551	0.0051%	619.72	49.8%
4	797,645	0.0066%	997.50	37.4%

Table 3 Iowa Accepted Individual District Metrics

The vertical line in subfigure (b) indicates the partisan slant of the entire whole. Democratic votes make up 46% of all votes cast, but 93 out of the 99 of counties have republican majorities, with the democratic majorities being by larger margins in fewer counties. As a result the counties themselves display a noticeable efficiency gap, but rather than attributing this to gerrymandering of county borders, it may be possible that socio-geographical phenomena (e.g., urban/rural divides) make it such that Democratic and Republican populations are generally distributed as such in the Iowa political geography, regardless of borders. This illustrates the importance of understanding partisan fairness metrics such as efficiency gap in terms of what is actually feasible in the given political geography, and in relation to the existence of other competing metrics.

The sub-objective values of our inverse inputs are detailed in Table 1. Population data is drawn from the 2020 Census and political data from the 2020 presidential election. We note that in both districtings, the evaluation of the efficiency gap is in favor of Republican over-representation. We also supply district-by-district measurements of the metrics that are used to calculate inverse inputs in Tables 2 and 3 for the rejected and accepted districting plans, respectively. For context we note that the ideal district population is 797,592 and the Iowa state perimeter is 1151 miles.

7.3. Inverse Optimization Analysis

Although Iowa is computationally easier than other larger states, coarsening and ensemble methods are still needed for tractability. We use our heavy ball descent method, in conjunction with an ensemble of 64 graphs, each coarsened from the original state data three times. For our preliminary inverse analysis of the state, we produce an ensemble of 64 coarsenings of the state using 3 rounds

Metric	Analysis 1 Objectives	Analysis 2 Objectives
Perimeter Compactness	0.055	0
Population Imbalance	0.933	1
Efficiency Gap	0.011	0
Reported Optimality Gap	-0.0014	-0.0014

Table 4 Iowa 2022 Rejected Districts Inverse Output

Metric	Analysis 1	Analysis 2
Perimeter Compactness	0	0
Population Imbalance	1	1
Efficiency Gap	0	0
Reported Optimality Gap	0.0772	0.0042

Table 5 Iowa 2022 Accepted Districts Inverse Output

of random maximal matching. Over this ensemble of coarsenings, we solve the $\text{MultiGIO}_{\text{abs}} \text{MinMax}$ multipoint formulation, using PGD-A for finding the optimality gap minimizer with the same parameters described in Section 6.3.1.

We conduct two inverse optimization analyses for the accepted and rejected districtings. In Analysis 1, we minimize the optimality gap for a objective weighting that is a combination of minimizing perimeter compactness (σ_P), population imbalance (ρ), and efficiency gap (ϕ_{EG}). In Analysis 2, we reformulate the efficiency gap metric so that the objective component represents *maximizing* efficiency gap in favor of the Republican party (which both districtings favor). Since the original efficiency gap objective is formulated as an absolute value of a quantity $\frac{\sum_{i \in V} w_i}{\sum_{i \in V} (p_i^D + p_i^R)}$ that is positive when it benefits Democrats and negative when it benefits Republicans (see equations (2p) and (2q)), we substitute ϕ_{EG} in the objective with this ‘directional’ quantity, and for our inverse input, the value of this quantity is equal to the negative efficiency gap. Minimizing this quantity is equivalent to maximizing the amount that the efficiency gap favors Republicans. We note that the linear dependence of the minimizing and maximizing ϕ_{EG} objectives makes it impossible for both subobjectives to be included in the same inverse analysis as the FOP objective feasible space might not have a fully dimensional feasible region. Thus by doing side-by-side analyses with both objectives and comparing the found optimality gaps, we can assess these objectives in comparison.

The results from both analyses are detailed in Tables 4 and 5 for the rejected and accepted districting plans, respectively. All analyses indicate that both districting plans place nearly all emphasis on minimizing population imbalance, with only the rejected districting placing some objective weight on minimizing perimeter compactness and partisan efficiency gap.

The interpretation of our inverse analyses of these two districtings is that the accepted districting prioritizes minimizing population imbalance with. This supports the hypothesis that the currently enacted Iowa districts are not intentionally gerrymandered to benefit the Republican party. However, the extra priority placed on minimizing the population imbalance between the rejected and

accepted plans in order to reduce imbalance by 16% also increases to the perimeter and efficiency gap metrics by 6% and 372% respectively. Thus, this may still raise questions and discussion as to whether sole focus on reducing population imbalance is necessary when it entails such costs to other democratic values, even if there is not explicit intent to gerrymander districts.

We note that alternative quantitative analysis methods in the literature often model equal population considerations in districtings through constraints that put an upper limit on the population imbalance in modeled districts; the ALARM Project (McCartan et al. 2022) simulates possible districts with an upper limit of 0.5% population imbalance, and Swamy et al. (2022) utilize an upper bound of 4.8% in analyzing possible district plans for Wisconsin. We note that our application of generalized inverse optimization methods allows for the addition of population imbalance as a metric to be considered as optimized in itself (whereas Swamy et al. (2022)’s method of plotting Pareto frontiers is not practical for considering more than two objectives at once). As such, our methods are able to bring new considerations that indicate that with this objective considered, Iowa’s districts may not be the result of prioritizing Republican advantage, whereas the ALARM Project’s simulation-based analysis that permits larger population imbalances indicates that the efficiency gap of the employed districting is anomalous to the point of being indicative of gerrymandering.

We note that the analysis of the rejected districting reports optimality gaps that are negative, which indicates that our inverse input objective values cannot be Pareto-dominated by any solution that is feasible for some element in our ensemble of coarsened graphs. Since the Iowa districting input is in fact a feasible districting, it should be possible that a more comprehensive inverse modeling analysis, either utilizing the full-sized graph of Iowa without any heuristic methods, or an analysis with larger ensembles and/or graphs that are coarsened to a lesser extent, could retrieve a solution with a non-negative reported optimality gap. However, if the Pareto frontier of the feasible region covered by our ensemble is reasonably similar to the geometry of the true forward problem Pareto frontier, then the results are still interpretable.

8. Conclusion

In summary, this paper makes three contributions. First, we propose a new approach for solving generalized mixed-integer IO problems based on sub-gradient methods. Second, we develop custom heuristic methods for graph-based inverse problems using a combination of graph coarsening and ensemble methods. Third, we propose a new application domain – quantitatively identifying gerrymandering – for generalized inverse integer optimization. We argue that IO can produce more nuanced data-driven arguments that proposed districtings should be considered gerrymandered.

Acknowledgments

The authors thank Professor Ian Zhu for providing insightful feedback and suggestions to improve this work.

References

- Ahuja, Ravindra K, James B Orlin. 2001. Inverse optimization. *Operations research* **49**(5) 771–783.
- Aswani, Anil, Zuo-Jun Shen, Auyon Siddiq. 2018. Inverse optimization with noisy data. *Operations Research* **66**(3) 870–892.
- Babier, Aaron, Timothy CY Chan, Taewoo Lee, Rafid Mahmood, Daria Terekhov. 2021. An ensemble learning framework for model fitting and evaluation in inverse linear optimization. *Informs Journal on Optimization* **3**(2) 119–138.
- Becker, Amariah, Moon Duchin, Dara Gold, Sam Hirsch. 2021. Computational redistricting and the voting rights act. *Election Law Journal: Rules, Politics, and Policy* **20**(4) 407–441. doi:10.1089/elj.2020.0704. URL <https://doi.org/10.1089/elj.2020.0704>.
- Bodur, Merve, Timothy CY Chan, Ian Yihang Zhu. 2022. Inverse mixed integer optimization: Polyhedral insights and trust region methods. *INFORMS Journal on Computing* .
- Boyd, Stephen, Lin Xiao, Almir Mutapcic. 2003. Subgradient methods. *lecture notes of EE392o, Stanford University, Autumn Quarter* **2004** 2004–2005.
- Breiman, Leo. 1996. Bagging predictors. *Machine learning* **24** 123–140.
- Bulut, Aykut, Ted K Ralphs. 2021. On the complexity of inverse mixed integer linear optimization. *SIAM Journal on Optimization* **31**(4) 3014–3043.
- Chan, Timothy CY, Tim Craig, Taewoo Lee, Michael B Sharpe. 2014. Generalized inverse multiobjective optimization with application to cancer therapy. *Operations Research* **62**(3) 680–695.
- Chan, Timothy CY, Taewoo Lee, Daria Terekhov. 2019. Inverse optimization: Closed-form solutions, geometry, and goodness of fit. *Management Science* **65**(3) 1115–1135.
- Chan, Timothy CY, Rafid Mahmood, Ian Yihang Zhu. 2023. Inverse optimization: Theory and applications. *Operations Research* .
- Chen, Jie, Ronny Luss. 2019. Stochastic gradient descent with biased but consistent gradient estimators.
- Daryl DeFord, Moon Duchin, Justin Solomon. 2020. A computational approach to measuring vote elasticity and competitiveness. *Statistics and Public Policy* **7**(1) 69–86. doi:10.1080/2330443X.2020.1777915. URL <https://doi.org/10.1080/2330443X.2020.1777915>.
- Duchin, Moon. 2018. Gerrymandering metrics: How to measure? what’s the baseline? *arXiv preprint arXiv:1801.02064* .
- Duchin, Moon, Taissa Gladkova, Eugene Henninger-Voss, Ben Klingensmith, Heather Newman, Hannah Wheelen. 2019. Locating the representational baseline: Republicans in massachusetts. *Election Law Journal: Rules, Politics, and Policy* **18**(4) 388–401. doi:10.1089/elj.2018.0537. URL <https://doi.org/10.1089/elj.2018.0537>.
- Frank, Marguerite, Philip Wolfe. 1956. An algorithm for quadratic programming **3**(1) 95–110. doi:10.1002/nav.3800030109. URL <https://onlinelibrary.wiley.com/doi/abs/10.1002/nav.3800030109>.

- Garfinkel, Robert S, George L Nemhauser. 1970. Optimal political districting by implicit enumeration techniques. *Management Science* **16**(8) B–495.
- Ghobadi, Kimia, Taewoo Lee, Houra Mahmoudzadeh, Daria Terekhov. 2018. Robust inverse optimization. *Operations Research Letters* **46**(3) 339–344.
- Gleixner, Ambros, Gregor Hendel, Gerald Gamrath, Tobias Achterberg, Michael Bastubbe, Timo Berthold, Philipp M. Christophel, Kati Jarck, Thorsten Koch, Jeff Linderoth, Marco Lübbecke, Hans D. Mittelmann, Derya Ozyurt, Ted K. Ralphs, Domenico Salvagnin, Yuji Shinano. 2021. MIPLIB 2017: Data-Driven Compilation of the 6th Mixed-Integer Programming Library. *Mathematical Programming Computation* doi:10.1007/s12532-020-00194-3. URL <https://doi.org/10.1007/s12532-020-00194-3>.
- Grofman, Bernard, Gary King. 2007. The future of partisan symmetry as a judicial test for partisan gerrymandering after *lulac v. perry*. *Election Law Journal* **6**(1) 2–35.
- Hess, Sidney Wayne, JB Weaver, HJ Siegfeldt, JN Whelan, PA Zitlau. 1965. Nonpartisan political redistricting by computer. *Operations Research* **13**(6) 998–1006.
- Iyengar, Garud, Wanmo Kang. 2005. Inverse conic programming with applications. *Operations Research Letters* **33**(3) 319–330.
- Keshavarz, Arezou, Yang Wang, Stephen Boyd. 2011. Imputing a convex objective function. *2011 IEEE international symposium on intelligent control*. IEEE, 613–619.
- King, Douglas M, Sheldon H Jacobson, Edward C Sewell. 2015. Efficient geo-graph contiguity and hole algorithms for geographic zoning and dynamic plane graph partitioning. *Mathematical Programming* **149**(1) 425–457.
- Lamperski, Jourdain B, Andrew J Schaefer. 2015. A polyhedral characterization of the inverse-feasible region of a mixed-integer program. *Operations Research Letters* **43**(6) 575–578.
- Lieb, David. 2022. Explainer: How supreme court case could alter us house seats. *The Associated Press* .
- McCartan, Cory, Christopher T Kenny, Tyler Simko, George Garcia III, Kevin Wang, Melissa Wu, Shiro Kuriwaki, Kosuke Imai. 2022. Simulated redistricting plans for the analysis and evaluation of redistricting in the united states. *Scientific Data* **9**(1) 689.
- Mehrotra, Anuj, Ellis L Johnson, George L Nemhauser. 1998. An optimization based heuristic for political districting. *Management Science* **44**(8) 1100–1114.
- Moghaddass, Mahsa, Daria Terekhov. 2020. Inverse integer optimization with an imperfect observation. *Operations Research Letters* **48**(6) 763–769.
- Nagle, John F. 2017. How competitive should a fair single member districting plan be? *Election Law Journal* **16**(1) 196–209.
- Patriksson, Michael. 2015. *The traffic assignment problem: models and methods*. Courier Dover Publications.
- Polyak, Boris T. 1964. Some methods of speeding up the convergence of iteration methods. *Ussr computational mathematics and mathematical physics* **4**(5) 1–17.

- Ricca, Federica, Andrea Scozzari, Bruno Simeone. 2013. Political districting: from classical models to recent approaches. *Annals of Operations Research* **204** 271–299.
- Schaefer, Andrew J. 2009. Inverse integer programming. *Optimization Letters* **3** 483–489.
- Schapire, Robert E. 1999. A brief introduction to boosting. *Ijcai*, vol. 99. Citeseer, 1401–1406.
- Schmidt, Mark. 2019. Cpsc 540: Machine learning lecture notes .
- Scroccaro, Pedro Zattoni, Bilge Atasoy, Peyman Mohajerin Esfahani. 2023. Learning in inverse optimization: Incenter cost, augmented suboptimality loss, and algorithms. *arXiv preprint arXiv:2305.07730* .
- Sherman, Mark. 2019. Supreme court allows partisan districts, blocks census query. *The Associated Press* .
- Stephanopoulos, Nicholas, Eric McGhee. 2018. The measure of a metric: The debate over quantifying partisan gerrymandering .
- Stephanopoulos, Nicholas O, Eric M McGhee. 2015. Partisan gerrymandering and the efficiency gap. *The University of Chicago Law Review* 831–900.
- Swamy, Rahul, Douglas M King, Sheldon H Jacobson. 2022. Multiobjective optimization for politically fair districting: A scalable multilevel approach. *Operations Research* .
- Validi, Hamidreza, Austin Buchanan, Eugene Lykhovyd. 2022. Imposing contiguity constraints in political districting models. *Operations Research* **70**(2) 867–892.
- Villeneuve, Marina. 2022. Fight over gerrymandering argued at new york’s highest court. *The Associated Press* .
- Wang, Lizhi. 2009. Cutting plane algorithms for the inverse mixed integer linear programming problem. *Operations research letters* **37**(2) 114–116.
- Wang, Lizhi. 2013. Branch-and-bound algorithms for the partial inverse mixed integer linear programming problem. *Journal of Global Optimization* **55**(3) 491–506.
- Young, H Peyton. 1988. Measuring the compactness of legislative districts. *Legislative Studies Quarterly* 105–115.
- Zhang, Jianzhong, Chengxian Xu. 2010. Inverse optimization for linearly constrained convex separable programming problems. *European Journal of Operational Research* **200**(3) 671–679.
- Zhao, Qi, Arion Stettner, Ed Reznik, Daniel Segrè, Ioannis Ch Paschalidis. 2015. Learning cellular objectives from fluxes by inverse optimization. *2015 54th IEEE Conference on Decision and Control (CDC)*. IEEE, 1271–1276.

Electronic Companion

EC.1. Proofs

EC.1.1. Proof of proposition 3

Proof of Proposition 3: Let $\xi_{ABS}^k(\alpha)$ denote the gap function corresponding to the inverse optimization model $\text{GIO}_{ABS}(\hat{\mathbf{y}}, \mathcal{S}^k)$. We note that that $\text{GIO}_{ABS}(\hat{\mathbf{y}}, \mathcal{S}^k)$ is a relaxation of $\text{GIO}_{ABS}(\hat{\mathbf{y}}, \mathcal{S})$, and as such $\xi_{ABS}^k(\alpha) \leq \xi_{ABS}(\alpha)$. We prove the claim by showing that if $\mathbf{C}\hat{\mathbf{y}} - \xi_{ABS}(\alpha^*)\mathbf{1} \in \text{conv}(B^k)$ then; (i) $\xi_{ABS}^k(\alpha^*) = \xi_{ABS}(\alpha)$, and (ii) $\xi_{ABS}^k(\alpha^*) < \xi_{ABS}^k(\alpha)$, $\forall \alpha \in \mathcal{A} \setminus \alpha^*$.

Proof of (i): Since $\mathbf{C}\hat{\mathbf{y}} - \xi_{ABS}(\alpha^*)\mathbf{1} \in \text{conv}(B^k)$, it is true that $\mathbf{C}\hat{\mathbf{y}} - \xi_{ABS}(\alpha^*)\mathbf{1} = \lambda_0\mathbf{C}\mathbf{y}^{(0)} + \lambda_1\mathbf{C}\mathbf{y}^{(1)} + \dots + \lambda_k\mathbf{C}\mathbf{y}^{(k)}$ for some $\lambda \in [0, 1]^k$, $\|\lambda\| = 1$. Thus we have,

$$\begin{aligned} \xi_{ABS}(\alpha^*) &= \alpha^{*\top}\mathbf{C}\hat{\mathbf{y}} - \min_{\mathbf{y} \in \mathcal{S}} \alpha^{*\top}\mathbf{C}\mathbf{y} \\ \alpha^{*\top}\mathbf{C}\hat{\mathbf{y}} - \alpha^{*\top}(\mathbf{C}\hat{\mathbf{y}} - \xi_{ABS}(\alpha^*)\mathbf{1}) &= \alpha^{*\top}\mathbf{C}\hat{\mathbf{y}} - \min_{\mathbf{y} \in \mathcal{S}} \alpha^{*\top}\mathbf{C}\mathbf{y} \\ \alpha^{*\top}\mathbf{C}\hat{\mathbf{y}} - \alpha^{*\top}(\lambda_0\mathbf{C}\mathbf{y}^{(0)} + \lambda_1\mathbf{C}\mathbf{y}^{(1)} + \dots + \lambda_k\mathbf{C}\mathbf{y}^{(k)}) &= \alpha^{*\top}\mathbf{C}\hat{\mathbf{y}} - \min_{\mathbf{y} \in \mathcal{S}} \alpha^{*\top}\mathbf{C}\mathbf{y} \\ \alpha^{*\top}(\lambda_0\mathbf{C}\mathbf{y}^{(0)} + \lambda_1\mathbf{C}\mathbf{y}^{(1)} + \dots + \lambda_k\mathbf{C}\mathbf{y}^{(k)}) &= \min_{\mathbf{y} \in \mathcal{S}} \alpha^{*\top}\mathbf{C}\mathbf{y} \end{aligned}$$

This implies that each $\mathbf{y}^{(i)} \in \mathcal{S}^k$ for which $\lambda_i > 0$ is a minimizer of $\min_{\mathbf{y} \in \mathcal{S}} \alpha^{*\top}\mathbf{C}\mathbf{y}$, i.e. it is an optimal solution of the multiobjective FOP with weight vector α^* . Since $\mathcal{S}^k \subseteq \mathcal{S}$, we then have,

$$\begin{aligned} \xi_{ABS}^k(\alpha^*) &= \alpha^{*\top}\mathbf{C}\hat{\mathbf{y}} - \min_{\mathbf{y} \in \mathcal{S}^k} \alpha^{*\top}\mathbf{C}\mathbf{y} \\ \xi_{ABS}^k(\alpha^*) &= \alpha^{*\top}\mathbf{C}\hat{\mathbf{y}} - \alpha^{*\top}(\lambda_0\mathbf{C}\mathbf{y}^{(0)} + \lambda_1\mathbf{C}\mathbf{y}^{(1)} + \dots + \lambda_k\mathbf{C}\mathbf{y}^{(k)}) \\ \xi_{ABS}^k(\alpha^*) &= \xi_{ABS}(\alpha^*) \end{aligned}$$

Proof of (ii): Let I denote the the set of indices $i \in 0 \dots k$ for which $\lambda_i > 0$. As stated above, this implies that each $\mathbf{y}^{(i)} \in \mathcal{S}^k$, $i \in I$ is a minimizer of $\min_{\mathbf{y} \in \mathcal{S}^k} \alpha^{*\top}\mathbf{C}\mathbf{y}$. For any $\alpha \in \mathcal{A} \setminus \alpha^*$, we may express α as $\alpha^* + \epsilon$ for some $\epsilon \in \mathbb{R}^{|\mathcal{K}|}$, $\epsilon^\top\mathbf{1} = 0$, $\epsilon \neq \mathbf{0}$. As such we have,

$$\begin{aligned} \xi_{ABS}^k(\alpha) &= \alpha^\top\mathbf{C}\hat{\mathbf{y}} - \min_{\mathbf{y} \in \mathcal{S}^k} \alpha^\top\mathbf{C}\mathbf{y} \\ \xi_{ABS}^k(\alpha) &= (\alpha^* + \epsilon)^\top\mathbf{C}\hat{\mathbf{y}} - \min_{\mathbf{y} \in \mathcal{S}^k} (\alpha^* + \epsilon)^\top\mathbf{C}\mathbf{y} \end{aligned}$$

Let $\bar{\mathbf{y}}$ denote $\min_{\mathbf{y} \in \mathcal{S}^k, i \in I} (\epsilon)^\top\mathbf{C}\mathbf{y}$. Since $\mathbf{C}\hat{\mathbf{y}} - \xi_{ABS}(\alpha^*)\mathbf{1}$ lies in the *interior* of a facet of $\text{conv}(B^k)$, then it must be true that there is a set of $|\mathcal{K}|$ linearly independent elements of $\mathbf{C}\mathbf{y}^{(i)} \in B^k$ such that $i \in I$. Let us denote this set \bar{B} . We note that $\text{conv}(\bar{B})$ is a subset of a facet of $\text{conv}(B^k)$, and that $\mathbf{C}\hat{\mathbf{y}} - \xi_{ABS}(\alpha^*)\mathbf{1}$ is contained in the interior of this subset. The elements of \bar{B} define a set of dimension $|\mathcal{K}| - 1$ contained in the plane $\alpha^{*\top}\mathbf{C}\mathbf{y} = (\min_{\mathbf{y} \in \mathcal{S}} \alpha^{*\top}\mathbf{C}\mathbf{y})$. Since the elements of \bar{B} are linearly independent and α^* and ϵ are not parallel vectors, it must be that there is at least one

element $\mathbf{C}\hat{\mathbf{y}} \in \bar{B}$ such that $\epsilon^\top \mathbf{C}\hat{\mathbf{y}} > \epsilon^\top \mathbf{C}\bar{\mathbf{y}}$. Then it must also be true that $\epsilon^\top \mathbf{C}\bar{\mathbf{y}} < \epsilon^\top (\sum_{i \in I} \lambda_i \mathbf{C}\mathbf{y}^{(i)}) = \epsilon^\top (\mathbf{C}\hat{\mathbf{y}} - \xi_{\text{ABS}}(\boldsymbol{\alpha}^*)\mathbf{1})$. With this, we then have that

$$\begin{aligned} \xi_{\text{ABS}}^k(\boldsymbol{\alpha}) &\geq \boldsymbol{\alpha}^{*\top} \mathbf{C}\hat{\mathbf{y}} - \boldsymbol{\alpha}^{*\top} \mathbf{C}\bar{\mathbf{y}} + \epsilon^\top \mathbf{C}\hat{\mathbf{y}} - \epsilon^\top \mathbf{C}\bar{\mathbf{y}} \\ \xi_{\text{ABS}}^k(\boldsymbol{\alpha}) &\geq \xi_{\text{ABS}}^k(\boldsymbol{\alpha}^*) + \epsilon^\top \mathbf{C}\hat{\mathbf{y}} - \epsilon^\top \mathbf{C}\bar{\mathbf{y}} \\ \xi_{\text{ABS}}^k(\boldsymbol{\alpha}) &> \xi_{\text{ABS}}^k(\boldsymbol{\alpha}^*) + \epsilon^\top \mathbf{C}\hat{\mathbf{y}} - \epsilon^\top (\mathbf{C}\hat{\mathbf{y}} - \xi_{\text{ABS}}(\boldsymbol{\alpha}^*)\mathbf{1}) \\ \xi_{\text{ABS}}^k(\boldsymbol{\alpha}) &> \xi_{\text{ABS}}^k(\boldsymbol{\alpha}^*) + (\epsilon^\top \mathbf{C}\hat{\mathbf{y}} - \epsilon^\top \mathbf{C}\bar{\mathbf{y}}) + \xi_{\text{ABS}}(\boldsymbol{\alpha}^*)\epsilon^\top \mathbf{1} \\ \xi_{\text{ABS}}^k(\boldsymbol{\alpha}) &> \xi_{\text{ABS}}^k(\boldsymbol{\alpha}^*) + \xi_{\text{ABS}}(\boldsymbol{\alpha}^*) * 0 \\ \xi_{\text{ABS}}^k(\boldsymbol{\alpha}) &> \xi_{\text{ABS}}^k(\boldsymbol{\alpha}^*) \end{aligned}$$

□

EC.1.2. Proof of proposition 4

Proof of proposition 4: In order to show that the algorithm terminates, we first demonstrate that the algorithm will always reach a termination check criterion in a finite number of iterations, until one such check succeeds. We first show that for any algorithm step k , either $\nabla \xi_{\text{ABS}}(\boldsymbol{\alpha}^{(k)}) = 0$ and the termination check will occur, or there exists a step $k+n$ such that $\boldsymbol{\alpha}^{(k+n)\top} \mathbf{C}\hat{\mathbf{y}} - \boldsymbol{\alpha}^{(k+n)\top} \mathbf{C}\mathbf{y}^{(k+n)} > \xi_{\text{ABS}} + (\boldsymbol{\alpha}^{(k+n)} - \boldsymbol{\alpha}^{(k+n-1)})^\top (\mathbf{C}(\hat{\mathbf{y}} - \mathbf{y}^{(k+n-1)}))$ and $\mathbf{y}^{(k+n)} \in \mathcal{S}^{(k+n-1)}$. At a given step k , $\boldsymbol{\alpha}^{(k)}$ is found on some facet of the gap function ξ_{ABS} defined by $\mathbf{y}^{(k)}$. If $\nabla \xi_{\text{ABS}}(\boldsymbol{\alpha}^{(k)}) \neq 0$, then the descent method will proceed to take identical steps until some $\boldsymbol{\alpha}^{(k+n)}$ either leaves said facet, in which case $\mathbf{y}^{(k+n)} \neq \mathbf{y}^{(k+n-1)}$, or arrives at the boundary of \mathcal{A} and $\boldsymbol{\alpha}^{(k+n)} = \boldsymbol{\alpha}^{(k+n-1)}$, at which point a termination check will occur. If $\boldsymbol{\alpha}^{(k+n)}$ leaves said facet, then $\mathbf{y}^{(k+n)} \neq \mathbf{y}^{(k+n-1)}$, and since the newfound facet has a different subgradient, the gap function will not decrease by the maximum amount, and thus $\boldsymbol{\alpha}^{(k+n)\top} \mathbf{C}\hat{\mathbf{y}} - \boldsymbol{\alpha}^{(k+n)\top} \mathbf{C}\mathbf{y}^{(k+n)} > \xi_{\text{ABS}} + (\boldsymbol{\alpha}^{(k+n)} - \boldsymbol{\alpha}^{(k+n-1)})^\top (\mathbf{C}(\hat{\mathbf{y}} - \mathbf{y}^{(k+n-1)}))$. Since $\text{conv}(\mathcal{S})$ has a finite number of extreme points, there exists some step $k+n$ where $\boldsymbol{\alpha}^{(k+n)\top} \mathbf{C}\hat{\mathbf{y}} - \boldsymbol{\alpha}^{(k+n)\top} \mathbf{C}\mathbf{y}^{(k+n)} > \xi_{\text{ABS}} + (\boldsymbol{\alpha}^{(k+n)} - \boldsymbol{\alpha}^{(k+n-1)})^\top (\mathbf{C}(\hat{\mathbf{y}} - \mathbf{y}^{(k+n-1)}))$ and $\mathbf{y}^{(k+n)} \in \mathcal{S}^{(k+n-1)}$. Thus, Algorithm 1 will always reach a termination check in a finite number of steps, and will continue to do so until one succeeds and terminates the algorithm.

Since each failed termination check must necessarily find a vertex of $\text{conv}(\mathcal{B})$ that is not in B^k and then adds it to B^{k+1} , and $\text{conv}(\mathcal{B})$ has a finite number of vertices, there must be a finite number of failed termination checks until one succeeds, and by Proposition 3, yields the correct solution. Thus, Algorithm 1 terminates in a finite number of steps. □

EC.1.3. Proof of theorem 1

Proof of Theorem 1: Let $\mathcal{B}_i = \{\mathbf{C}\mathbf{y}, \forall \mathbf{y} \in \mathcal{S}_i\}$. Since ξ_{ENS} lower bounds ξ_{ABS} , we have by Proposition 3 that if $\mathcal{B}_1 \cup \mathcal{B}_2 \cup \dots \cup \mathcal{B}_n$ contains a set \bar{B} of values of $\mathbf{C}\mathbf{y}$ whose convex hull contains

$\mathbf{C}\hat{\mathbf{y}} - \xi_{\text{ABS}}(\boldsymbol{\alpha}^*)$, then ξ_{ENS} and ξ_{ABS} will have the same minimum value and minimizer. We also know from Proposition 3 that there exists some set \bar{B} with a total of $|\mathcal{K}|$ elements. Each $\mathbf{C}\mathbf{y} \in \bar{B}$ is the objective vector of a given partitioning of G into k districts. We note that if the i^{th} coarsening of a graph $G = \{V, E\}$ does not contract any edges in the edge cut of said districting, then there is a feasible solution to FOP_i that corresponds to the same districting. Since any such districting is a subgraph of G with L disjoint connected components that covers V , there are at least $|V| - L$ edges in E do not traverse the edge cut. Further any coarsening of G down to v vertices must contract exactly $|V| - v$ edges. Thus, if $v \geq L$ there exists at least one way of coarsening G such that no edges in the edge cut are contracted. Assuming that our ensemble generation method has a non-zero probability of generating any possible coarsening of G down to v vertices for any coarsening, then for any $\mathbf{C}\mathbf{y} \in \bar{B}$ and any coarsening i in our ensemble, $\text{Prob}(\mathbf{C}\mathbf{y} \notin \mathcal{B}_i) < 1$. If each coarsening in our ensemble is independently sampled, then as $n \rightarrow \infty$:

$$\text{Prob}(\mathbf{C}\mathbf{y} \notin \mathcal{B}_1 \cup \mathcal{B}_2 \cup \dots \cup \mathcal{B}_n) = \prod_{i \in 1 \dots n} \text{Prob}(\mathbf{C}\mathbf{y} \notin \mathcal{B}_i) \rightarrow 0$$

Since $\text{Prob}(\bar{B} \not\subseteq \mathcal{B}_1 \cup \mathcal{B}_2 \cup \dots \cup \mathcal{B}_n) = \text{Prob}(\bigcup_{\mathbf{b} \in \bar{B}} (\mathbf{b} \notin \mathcal{B}_1 \cup \mathcal{B}_2 \cup \dots \cup \mathcal{B}_n))$, we also have that as $n \rightarrow \infty$, $\text{Prob}(\bar{B} \not\subseteq \mathcal{B}_1 \cup \mathcal{B}_2 \cup \dots \cup \mathcal{B}_n) \rightarrow 0$. \square

EC.1.4. Proof of proposition 5

Proof of Proposition 5: If we can find a subtangent plane of $\xi_{\text{ENS}}(\boldsymbol{\alpha})$ at $\boldsymbol{\alpha}^{(k)}$, then the gradient of said plane is a subgradient of $\xi_{\text{ENS}}(\boldsymbol{\alpha})$. Let us define our subtangent plane at $\boldsymbol{\alpha}^{(k)}$ as $P(\boldsymbol{\alpha}) = \boldsymbol{\alpha}^\top \mathbf{C}\hat{\mathbf{y}} - \boldsymbol{\alpha}^\top \mathbf{C}(\arg \min_{\mathbf{y} \in \mathbf{y}_1^{(k)} \dots \mathbf{y}_n^{(k)}} \boldsymbol{\alpha}^{(k)\top} \mathbf{C}\mathbf{y})$. Then, $\nabla P(\boldsymbol{\alpha}) = \mathbf{C}(\hat{\mathbf{y}} - \arg \min_{\mathbf{y} \in \mathbf{y}_1^{(k)} \dots \mathbf{y}_n^{(k)}} (\boldsymbol{\alpha}^{(k)\top} \mathbf{C}\mathbf{y}))$. To show that $P(\boldsymbol{\alpha})$ is subtangent at $\boldsymbol{\alpha}^{(k)}$, we show that (i) $P(\boldsymbol{\alpha}^{(k)}) = \xi_{\text{ENS}}(\boldsymbol{\alpha}^{(k)})$, and (ii) $P(\boldsymbol{\alpha}) \leq \xi_{\text{ENS}}(\boldsymbol{\alpha})$.

Proof of (i): we note by the formulation of $\text{MultiGIO}_{\text{ABS}}\text{MinMax}$ that $\xi_{\text{ENS}}(\boldsymbol{\alpha}) = \max_{i \in 1 \dots n} \xi_i(\boldsymbol{\alpha})$ where $\xi_i(\boldsymbol{\alpha})$ denotes the gap function generated by the inverse formulation GIO_{ABS} applied to FOP_i . Then we have that:

$$\begin{aligned} \xi_{\text{ENS}}(\boldsymbol{\alpha}) &= \max_{i \in 1 \dots n} \xi_i(\boldsymbol{\alpha}) \\ \xi_{\text{ENS}}(\boldsymbol{\alpha}) &= \max_{i \in 1 \dots n} (\boldsymbol{\alpha}^\top \mathbf{C}\hat{\mathbf{y}} - \min_{\mathbf{y} \in \mathcal{S}_i} \boldsymbol{\alpha}^\top \mathbf{C}\mathbf{y}) \end{aligned}$$

By Proposition 2, we have that:

$$\begin{aligned} \xi_{\text{ENS}}(\boldsymbol{\alpha}^{(k)}) &= \max_{i \in 1 \dots n} (\boldsymbol{\alpha}^{(k)\top} \mathbf{C}\hat{\mathbf{y}} - \boldsymbol{\alpha}^{(k)\top} \mathbf{C}\mathbf{y}_i^{(k)}) \\ \xi_{\text{ENS}}(\boldsymbol{\alpha}^{(k)}) &= \boldsymbol{\alpha}^{(k)\top} \mathbf{C}\hat{\mathbf{y}} - \boldsymbol{\alpha}^{(k)\top} \mathbf{C}(\arg \min_{\mathbf{y} \in \mathbf{y}_1^{(k)} \dots \mathbf{y}_n^{(k)}} \boldsymbol{\alpha}^{(k)\top} \mathbf{C}\mathbf{y}) \\ \xi_{\text{ENS}}(\boldsymbol{\alpha}^{(k)}) &= P(\boldsymbol{\alpha}^{(k)}) \end{aligned}$$

Proof of (ii):

$$\begin{aligned}\xi_{\text{ENS}}(\boldsymbol{\alpha}) &= \max_{i \in 1 \dots n} (\boldsymbol{\alpha}^\top \mathbf{C} \hat{\mathbf{y}} - \min_{\mathbf{y} \in \mathcal{S}_i} \boldsymbol{\alpha}^\top \mathbf{C} \mathbf{y}) \\ \xi_{\text{ENS}}(\boldsymbol{\alpha}) &= \boldsymbol{\alpha}^\top \mathbf{C} \hat{\mathbf{y}} - \min_{\mathbf{y} \in \mathcal{S}_1 \dots \mathcal{S}_n} \boldsymbol{\alpha}^\top \mathbf{C} \mathbf{y} \\ \xi_{\text{ENS}}(\boldsymbol{\alpha}) &\geq \boldsymbol{\alpha}^\top \mathbf{C} \hat{\mathbf{y}} - \boldsymbol{\alpha}^\top \mathbf{C} (\arg \min_{\mathbf{y} \in \mathbf{y}_1^{(k)} \dots \mathbf{y}_n^{(k)}} \boldsymbol{\alpha}^{(k)\top} \mathbf{C} \mathbf{y}) \\ \xi_{\text{ENS}}(\boldsymbol{\alpha}) &\geq P(\boldsymbol{\alpha})\end{aligned}$$

□

EC.2. Relative sub-optimality loss function

The relative sub-optimality loss function, $\ell_{\text{rel}}(\hat{\mathbf{y}}, \mathcal{S}, \boldsymbol{\alpha}) = \frac{\boldsymbol{\alpha}^\top \mathbf{C} \hat{\mathbf{y}}}{\min_{\mathbf{y} \in \mathcal{S}} \boldsymbol{\alpha}^\top \mathbf{C} \mathbf{y}}$ measures the quotient of the input solution objective value and the optimal objective value. We note that this loss function is well defined only if $\boldsymbol{\alpha} \in \mathbb{R}_+^{|\mathcal{K}|} \setminus \{\mathbf{0}\}$ and $\mathbf{C} \mathbf{y} > \mathbf{0}, \forall \mathbf{y} \in \mathcal{S}$. The corresponding data-driven inverse optimization problem with relative sub-optimality as a loss function can equivalently be written as:

$$\begin{aligned}\underset{\boldsymbol{\alpha}, \xi_{\text{rel}}}{\text{minimize}} \quad & \xi_{\text{rel}} && (\text{GIO}_{\text{rel}}) \\ \text{subject to} \quad & \boldsymbol{\alpha}^\top \mathbf{C} \hat{\mathbf{y}} \leq (\boldsymbol{\alpha}^\top \mathbf{C} \mathbf{y}) \xi_{\text{rel}}, \quad \forall \mathbf{y} \in \mathcal{S}, \\ & \boldsymbol{\alpha} \in \mathcal{A}, \\ & \boldsymbol{\alpha} \geq \mathbf{0}.\end{aligned}$$

Note that GIO_{rel} is not a linear program because two continuous decision variables are multiplied ($\boldsymbol{\alpha}$ and ξ_{rel}) in the first set of constraints. Chan et al. (2014) solve a similar formulation by varying ξ_{rel} with a univariate search technique until the smallest value for ξ is found such that GIO_{rel} is feasible. However in the case that \mathcal{A} is defined as the unit simplex, using a method similar to Chan et al. (2019), the exact minimum relative gap and corresponding objective weighting can be derived quickly from the solution of a single linear program.

THEOREM EC.1. $\{\bar{\boldsymbol{\alpha}}, \bar{\xi}_{\text{rel}}\}$ is an optimal solution to $(\text{GIO}_{\text{rel}})$ if $\bar{\boldsymbol{\alpha}} = \frac{\hat{\boldsymbol{\alpha}}}{\|\hat{\boldsymbol{\alpha}}\|_1}$ and $\bar{\xi}_{\text{rel}} = \hat{\boldsymbol{\alpha}}^\top \mathbf{C} \hat{\mathbf{y}}$, where $\hat{\boldsymbol{\alpha}}$ is an optimal solution to the following linear program $(\text{GIO}_{\text{rel}}^*)$:

$$\begin{aligned}\underset{\boldsymbol{\alpha}}{\text{minimize}} \quad & \boldsymbol{\alpha}^\top \mathbf{C} \hat{\mathbf{y}} && (\text{GIO}_{\text{rel}}^*) \\ \text{subject to} \quad & \boldsymbol{\alpha}^\top \mathbf{C} \mathbf{y} \geq 1, \quad \forall \mathbf{y} \in \mathcal{S}, \\ & \boldsymbol{\alpha} \geq \mathbf{0}.\end{aligned}$$

Proof of Theorem EC.1: First, we show that (i) $\{\bar{\boldsymbol{\alpha}}, \bar{\xi}_{\text{rel}}\}$ is a feasible solution to $(\text{GIO}_{\text{rel}})$. Next, we show that (ii) if $\{\bar{\boldsymbol{\alpha}}, \bar{\xi}_{\text{rel}}\}$ is not optimal for $(\text{GIO}_{\text{rel}})$, then $\hat{\boldsymbol{\alpha}}$ is not optimal for $(\text{GIO}_{\text{rel}}^*)$, thus proving the claim by contrapositive.

(i) We observe that $\|\bar{\alpha}\|_1 = 1$ and $\bar{\alpha} \geq \mathbf{0}$ by the construction of $\bar{\alpha}$ and $\bar{\xi}_{\text{rel}} = \hat{\alpha}^\top C \hat{\mathbf{y}} \geq 0$ because $C \hat{\mathbf{y}} \in \mathbb{R}_+^{|\mathcal{K}|}$. The remaining constraints are satisfied because $\forall \mathbf{y} \in \mathcal{S}$:

$$\bar{\alpha}^\top C \hat{\mathbf{y}} = \frac{\hat{\alpha}^\top C \hat{\mathbf{y}}}{\|\hat{\alpha}\|_1} = \frac{\bar{\xi}_{\text{rel}}}{\|\hat{\alpha}\|_1} \leq (\hat{\alpha}^\top C \mathbf{y}) \frac{\bar{\xi}_{\text{rel}}}{\|\hat{\alpha}\|_1} = \frac{\hat{\alpha}^\top C \mathbf{y}}{\|\hat{\alpha}\|_1} \bar{\xi}_{\text{rel}} = (\bar{\alpha}^\top C \mathbf{y}) \bar{\xi}_{\text{rel}}.$$

(ii) Suppose there exists a feasible solution $\{\alpha^*, \xi_{\text{rel}}^*\}$ to $(\text{GIO}_{\text{rel}})$ such that $\xi_{\text{rel}}^* < \bar{\xi}_{\text{rel}}$, i.e. $\{\bar{\alpha}, \bar{\xi}_{\text{rel}}\}$ is not an optimal solution. Let $\tilde{\alpha} = \frac{\xi_{\text{rel}}^* \alpha^*}{\alpha^{*\top} C \hat{\mathbf{y}}}$. Then, $\tilde{\alpha}$ is a feasible solution to $(\text{GIO}_{\text{rel}}^*)$ because $\tilde{\alpha} \geq \mathbf{0}$ and $\forall \mathbf{y} \in \mathcal{S}$:

$$\tilde{\alpha}^\top C \mathbf{y} = \frac{\xi_{\text{rel}}^*}{\alpha^{*\top} C \hat{\mathbf{y}}} (\alpha^{*\top} C \mathbf{y}) \geq \frac{\xi_{\text{rel}}^*}{\alpha^{*\top} C \hat{\mathbf{y}}} \frac{\alpha^{*\top} C \hat{\mathbf{y}}}{\xi_{\text{rel}}^*} = 1.$$

Since $\tilde{\alpha}^\top C \hat{\mathbf{y}} = \xi_{\text{rel}}^* < \bar{\xi}_{\text{rel}} = \hat{\alpha}^\top C \hat{\mathbf{y}}$, $\hat{\alpha}$ is not an optimal solution to $(\text{GIO}_{\text{rel}}^*)$, which contradicts the definition of $\hat{\alpha}$. Therefore, such an $\{\alpha^*, \xi_{\text{rel}}^*\}$ cannot exist, so $\{\bar{\alpha}, \bar{\xi}_{\text{rel}}\}$ must be an optimal solution for $(\text{GIO}_{\text{rel}})$. \square

Theorem EC.1 shows that we can obtain the optimal solution to GIO_{rel} (which is bilinear) by solving $\text{GIO}_{\text{rel}}^*$ (which is a linear program).

As such, our modification to the algorithm proposed by Moghaddass and Terekhov (2020) minimizes the relative sub-optimality loss function, rather than absolute sub-optimality. The algorithm structure is shown in Algorithm 2. The main distinction is that our algorithm solves $\text{GIO}_{\text{rel}}^*$ and uses Theorem EC.1 to obtain the solution to GIO_{rel} .

THEOREM EC.2. *Algorithm 2 terminates finitely with an optimal solution to GIO_{rel} .*

Proof of Theorem EC.2: The proof follows directly from the proof of termination and correctness in Moghaddass and Terekhov (2020), together with the proof of Theorem EC.1. \square

Theorem EC.2 demonstrates that Algorithm 2 produces the optimal solution to GIO_{rel} when the complete forward problem feasible region is known, in at most as many steps as there are extreme points to the forward multi-objective feasible region.

EC.3. Adapting gap-gradient methods to the relative sub-optimality loss function

In the case of the relative optimality gap, we apply gap-gradient methods to an inverse formulation based on the linearization $\text{GIO}_{\text{REL}}^*$. Thus, for relative gap problems, we can formulate the corresponding gap function as $\xi_{\text{REL}}(\alpha) = \alpha^\top C \hat{\mathbf{y}}$ defined over the gap function domain $\mathcal{A} = \{\alpha \in \mathbb{R}^{\mathcal{K}} \mid \alpha^\top C \mathbf{y} \geq 1, \alpha \geq 0, \forall \mathbf{y} \in \mathcal{S}\}$

Similar to the absolute gap case, we note that the feasible region of the master problem $\text{GIO}_{\text{rel}}^*$ in the case where all extreme points are known is the epigraph of the relative gap function, and we obtain the following result.

PROPOSITION EC.1. *The relative gap function $\xi_{\text{REL}}(\alpha)$ is a convex function.*

Algorithm 2: Data-driven relative gap cutting-plane method.

```

input :  $C, \mathbf{y}^0, \text{FP}$ 
output:  $\boldsymbol{\alpha}^{\text{best}}, \xi_{\text{rel}}^{\text{best}}$ 
 $\tilde{\mathcal{S}} \leftarrow \emptyset, \hat{\boldsymbol{\alpha}} \leftarrow \text{GenInvOp}_{\text{rel}}^*(\mathbf{y}^0, \tilde{\mathcal{S}});$ 
 $\boldsymbol{\alpha} \leftarrow \frac{\hat{\boldsymbol{\alpha}}}{\|\hat{\boldsymbol{\alpha}}\|_1}, \mathbf{y} \leftarrow \text{FP}(\boldsymbol{\alpha});$ 
 $\xi_{\text{rel}}^{\text{best}} \leftarrow \boldsymbol{\alpha}^\top C \mathbf{y}^0 - \boldsymbol{\alpha}^\top C \mathbf{y}, \boldsymbol{\alpha}^{\text{best}} \leftarrow \boldsymbol{\alpha};$ 
while  $\boldsymbol{\alpha}^\top C \mathbf{y}^0 > \boldsymbol{\alpha}^\top C \mathbf{y}$  do
   $\tilde{\mathcal{S}} \leftarrow \tilde{\mathcal{S}} \cup \mathbf{y};$ 
   $\hat{\boldsymbol{\alpha}} \leftarrow \text{GenInvOp}_{\text{rel}}^*(\mathbf{y}^0, \tilde{\mathcal{S}});$ 
   $\boldsymbol{\alpha} \leftarrow \frac{\hat{\boldsymbol{\alpha}}}{\|\hat{\boldsymbol{\alpha}}\|_1};$ 
   $\mathbf{y} \leftarrow \text{FP}(\boldsymbol{\alpha});$ 
  if  $\boldsymbol{\alpha}^\top C \mathbf{y}^0 - \boldsymbol{\alpha}^\top C \mathbf{y} = \xi_{\text{rel}}^{\text{best}}$  then
    if  $\boldsymbol{\alpha} = \boldsymbol{\alpha}^{\text{best}}$  then
      | stop
    else
      |  $\boldsymbol{\alpha}^{\text{best}} \leftarrow \boldsymbol{\alpha};$ 
    end
    if  $\boldsymbol{\alpha}^\top C \mathbf{y}^0 - \boldsymbol{\alpha}^\top C \mathbf{y} < \xi_{\text{abs}}^{\text{best}}$  then
      |  $\xi_{\text{abs}}^{\text{best}} \leftarrow \boldsymbol{\alpha}^\top C \mathbf{y}^0 - \boldsymbol{\alpha}^\top C \mathbf{y};$ 
      |  $\boldsymbol{\alpha}^{\text{best}} \leftarrow \boldsymbol{\alpha};$ 
    end
  end
end
end

```

Proof of Theorem EC.1: The gap function is a linear function, and as such is convex if its domain is convex. The domain of the gap function is the union of half-planes, and as such, is convex. \square

Figure EC.1(b) displays the domain of ξ_{REL} for an example inverse optimization problem with two objectives, and the vector $C\hat{\mathbf{y}}$ which is equal to the gradient of the gap function $\nabla \xi_{\text{REL}}(\boldsymbol{\alpha})$. Minimizing the gap function yields the minimizer $\boldsymbol{\alpha}^*$.

REMARK EC.1. Under the formulation of the relative gap space and relative gap function, each FOP extreme point $\mathbf{y}^{(k)}$ does not yield a tangent plane, but a facet of the boundary of the domain of the relative gap function. For the relative gap function the gradient is in fact uniform ($\nabla g_{\text{REL}}(\boldsymbol{\alpha}^{(k)}) = C\hat{\mathbf{y}}, \forall \boldsymbol{\alpha}^{(k)}$ in the interior of the relative gap function's domain), but each facet gained from an extreme point can be used to find the projection of the gradient onto the boundary of the relative gap function domain at that point. Specifically, for a facet-defining boundary plane $\boldsymbol{\alpha}^\top C \mathbf{y}^{(k)} = 1$ discovered by solving the forward problem at objective weighting $\boldsymbol{\alpha}^{(k)}$, the gradient

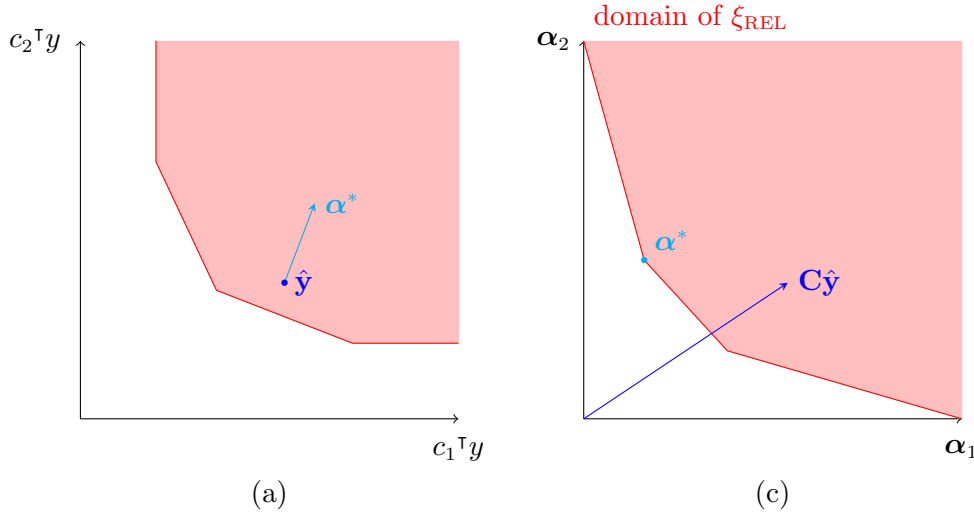


Figure EC.1 An example inverse optimization problem with two sub-objectives. (a) The FOP objective feasible space and inverse input $\hat{\mathbf{y}}$, and (b) the corresponding relative gap function projected onto two dimensions, and the gradient of the gap function $\nabla \xi_{\text{REL}}(\alpha) = C\hat{\mathbf{y}}$.

projected onto this boundary is $(\nabla g_{\text{REL}}(\alpha^{(k)}))_{\text{proj}} = C\hat{\mathbf{y}} - \left(\frac{(C\hat{\mathbf{y}})^\top C\mathbf{y}^{(k)}}{\|C\mathbf{y}^{(k)}\|_2^2}\right)C\mathbf{y}^{(k)}$. Similar to the absolute sub-optimality loss function, this can be used to minimize the convex relative gap function in a bounded space.

A gap-gradient solution method that uses this subgradient could proceed at each iteration by taking a step in the direction of the projected gradient. While it is possible that the $\alpha^{(k)}$ generated by this step lies outside of the domain \mathcal{A} due to incomplete knowledge of its boundary, we note that so long as $\alpha^{(k)}$ lies within the positive orthant, solving $\text{FOP}(\alpha^{(k)})$ will yield the same solution $\mathbf{y}^{(k)}$ as an FOP with some scalar-multiplied objective weight $m\alpha^{(k)}$, $m > 1$ such that $m\alpha^{(k)} \in \mathcal{A}$. Once $\mathbf{y}^{(k)}$ is known then the fact-defining plane $\alpha^\top C\mathbf{y}^{(k)} = 1$ can be used to project $\alpha^{(k)}$ onto the domain boundary by way of the projection $m = \frac{1}{\alpha^{(k)\top} C\mathbf{y}^{(k)}}$. One can then proceed in the gap-gradient algorithm by taking a step from $m\alpha^{(k)}$ in the direction of the next projected (negative) gradient, $-C\hat{\mathbf{y}} + \left(\frac{(C\hat{\mathbf{y}})^\top C\mathbf{y}^{(k)}}{\|C\mathbf{y}^{(k)}\|_2^2}\right)C\mathbf{y}^{(k)}$.

EC.4. Frank-Wolfe gap gradient methods with FOP early stopping

To operationalize this method of applying early stopping to solving the FOP when sufficient information is known, we can use the following approach. First, we create $|\mathcal{K}|$ different variations of the forward problem, each with an additional set of constraints $C_k(\mathbf{y} - \hat{\mathbf{y}}) \leq C_l(\mathbf{y} - \hat{\mathbf{y}})$, $\forall l \in 1 \dots \mathcal{K} \setminus k$, which enforces that subobjective component k of any feasible solution minus that of the input solution must be less than or equal to that of every other subobjective component. Figure EC.2 illustrates the FOP variations created by these constraints for the example two-objective inverse optimization problem shown in Figure 1 (a). Next, we solve each of the FOP_k , $k \in \mathcal{K}$ in parallel.

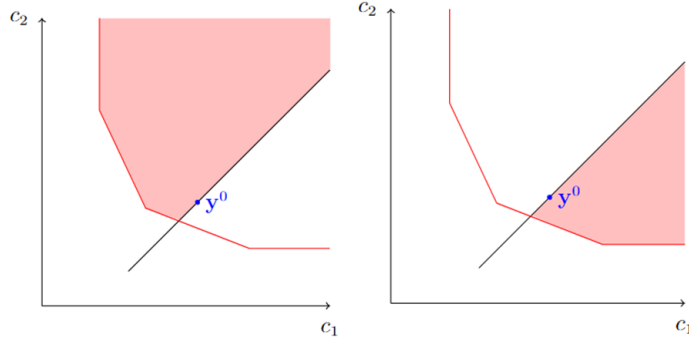


Figure EC.2 The feasible regions of two concurrently partially solved variations of the FOP shown in Figure 1 (a), used in conjunction with the proposed Frank-Wolfe method for potentially faster descent steps.

Once we reach a point where the lower objective bound of a given FOP_{*j*}, $j \in \mathcal{K}$, is greater than the lowest upper bound of any other running FOP_{*k*}, we can terminate the solving process of FOP_{*j*}. When only one such FOP_{*k*} remains, we terminate because it is unnecessary to solve to optimality because we know that whatever the optimal solution is, the gradient will have subobjective *k* as its greatest component, which is sufficient information to execute the next step in algorithm (the next descent step is in the direction towards e_k). This concurrent solving subalgorithm is detailed in the Appendix as Algorithm 6.

Using this method, we can also, at the point of terminating the final running subproblem, return the incumbent solution at the time of termination. This returns a feasible forward solution that produces a lower-bounding plane of the gap function. If it is an interior point, then it will not be tangent to the gap function, but strictly below. However, as our Frank-Wolfe method approaches α^* , the concurrent process will be terminating in smaller and smaller FOP optimality gaps, so the returned incumbents will be progressively closer to the boundary of $\text{conv}(\mathcal{B})$. Thus, once we are within a close neighborhood of the gap function minimizer, we may collect a set of proper tangent planes (at this point our method is likely to be returning vertices of $\text{conv}(\mathcal{B})$), and we can use these gathered tangent planes in a termination check that is similar to the termination methods used for our other proposed methods. The methods discussed in this section currently remain unimplemented because they will likely involve constructing an MILP solver from the ground up.

EC.5. Formulation.

The overall mixed-integer linear formulation for the FOP is given by:

$$\begin{array}{ll} \underset{x, z^D, v^D, f, \rho, \sigma_A, \phi_{EG}}{\text{minimize}} & \alpha_1 \rho + \alpha_2 \sigma_A + \alpha_3 \phi_{EG} \end{array} \quad (\text{EC.1a})$$

$$\text{subject to} \quad \sum_{i \in V} x_{ii} = L, \quad (\text{EC.1b})$$

$$\sum_{i \in V} x_{ij} = 1, \quad \forall j \in V, \quad (\text{EC.1c})$$

$$x_{ij} \leq x_{ii}, \quad \forall i, j \in V, \quad (\text{EC.1d})$$

$$x_{ij} + \sum_{v \in N(j)} (f_{ijv} - f_{ivj}) = 0, \quad \forall i, j \in V, i \neq j, \quad (\text{EC.1e})$$

$$x_{ii} + \sum_{v \in N(i)} (f_{iiv} - f_{ivi}) - \sum_{v \in N(i)} x_{iv} = 0, \quad \forall i \in V, \quad (\text{EC.1f})$$

$$|V|x_{ij} - \sum_{v \in N(j)} f_{ivj} \geq 0, \quad \forall i, j \in V, \quad (\text{EC.1g})$$

$$(x_{ii} - \rho)\bar{P} \leq \sum_{j \in V} p_j x_{ij}, \quad \forall i \in V, \quad (\text{EC.1h})$$

$$(x_{ii} + \rho)\bar{P} \geq \sum_{j \in V} p_j x_{ij}, \quad \forall i \in V, \quad (\text{EC.1i})$$

$$\sigma_A = \frac{\sum_{i, j \in V} d_{ij} a_j x_{ij}}{M}, \quad (\text{EC.1j})$$

$$\bar{P} \leq \sum_{j \in V} (p_j^D - p_j^R) x_{ij}, -\bar{P} z_i^D \leq 0, \quad \forall i \in V, \quad (\text{EC.1k})$$

$$v_{ij}^D \leq x_{ij}, \quad \forall i, j \in V, \quad (\text{EC.1l})$$

$$v_{ij}^D \leq z_i^D, \quad \forall i, j \in V, \quad (\text{EC.1m})$$

$$v_{ij}^D \geq x_{ij} + z_i^D - 1, \quad \forall i, j \in V, \quad (\text{EC.1n})$$

$$\sum_{j \in V} \left(\frac{3p_j^D - p_j^R}{2} \right) x_{ij} - \sum_{j \in V} (p_j^D + p_j^R) v_{ij}^D = w_i, \quad \forall i \in V, \quad (\text{EC.1o})$$

$$\phi_{EG} \geq \frac{\sum_{i \in V} w_i}{\sum_{i \in V} (p_i^D + p_i^R)}, \quad (\text{EC.1p})$$

$$\phi_{EG} \geq -\frac{\sum_{i \in V} w_i}{\sum_{i \in V} (p_i^D + p_i^R)}, \quad (\text{EC.1q})$$

$$x_{ij}, z_i^D, v_{ij}^D \in \{0, 1\}, f_{ivj} \geq 0, \quad \forall i, j \in V, \forall v \in N(j). \quad (\text{EC.1r})$$

Constraints (2b) through (2d) enforce that every vertex is assigned to exactly one district out of L total districts. Constraints (2e) through (2g) construct a set of flow networks that maintain contiguity for the created districts. Constraints (2h) and (2i) define the ρ variable used in the objective. Constraint (2j) defines σ_A (used in the objective). Finally, Constraints (2k) - (2q) define ϕ_{EG} , which is used in the objective.

EC.6. Experimental details

EC.6.1. MIPLIB instances

The following are labels for the FOPs used in Section 5:

1. neos-1430701
2. gsvm2r13

3. ran13x13
4. spd150x300d
5. supportcase17
6. ci-24
7. ic97_tension
8. fastxgemm-n2r60t2
9. timtab1CUTS

EC.6.2. Generating sample states

To create a sample state G for a specified $|V|$, we randomly sample $|V|$ points uniformly over a unit square, and calculate the Delaunay triangulation to create an adjacency graph of our simulated census blocks. The distance matrix is calculated using the euclidean distances of the sampled points. Note that scaling of the distance matrix does not matter, as the compactness metric of a districting is normalized for the 1-median of the entire state. Land areas for the corresponding simulated census blocks are calculated as the areas of the Voronoi cells produced by the sampled points. At each census block, values for the number of voters for party A, party B, and non-voting people are randomly sampled from integers in the range $[10, 100]$. For each sampled state, an FOP is generated for the political districting optimization model with $L = 2$ districts.

EC.7. Algorithm Structures

Algorithm 3: Moghaddass and Terekhov (2020)

```

input :  $\mathbf{C}, \hat{\mathbf{y}}, \text{FOP}$ 
output:  $\alpha^{\text{best}}, \xi^{\text{best}}$ 
 $\tilde{\mathcal{S}} \leftarrow \emptyset, \alpha \leftarrow \text{GIO}_{\text{ABS}}(\hat{\mathbf{y}}, \tilde{\mathcal{S}}), \mathbf{y} \leftarrow \text{FOP}(\alpha);$ 
 $\xi^{\text{best}} \leftarrow \alpha^\top \mathbf{C} \hat{\mathbf{y}} - \alpha^\top \mathbf{C} \mathbf{y}, \alpha^{\text{best}} \leftarrow \alpha;$ 
while  $\alpha^\top \mathbf{C} \hat{\mathbf{y}} > \alpha^\top \mathbf{C} \mathbf{y}$  do
     $\tilde{\mathcal{S}} \leftarrow \tilde{\mathcal{S}} \cup \mathbf{y};$ 
     $\alpha \leftarrow \text{GIO}_{\text{ABS}}(\hat{\mathbf{y}}, \tilde{\mathcal{S}});$ 
     $\mathbf{y} \leftarrow \text{FP}(\alpha);$ 
    if  $\alpha^\top \mathbf{C} \hat{\mathbf{y}} - \alpha^\top \mathbf{C} \mathbf{y} = \xi^{\text{best}}$  then
        if  $\alpha = \alpha^{\text{best}}$  then
            | stop
        else
            |  $\alpha^{\text{best}} \leftarrow \alpha;$ 
        end
        if  $\alpha^\top \mathbf{C} \hat{\mathbf{y}} - \alpha^\top \mathbf{C} \mathbf{y} < \xi_{\text{abs}}^{\text{best}}$  then
            |  $\xi_{\text{abs}}^{\text{best}} \leftarrow \alpha^\top \mathbf{C} \hat{\mathbf{y}} - \alpha^\top \mathbf{C} \mathbf{y};$ 
            |  $\alpha^{\text{best}} \leftarrow \alpha;$ 
        end
    end
end

```

Algorithm 4: Gap-gradient Projected Gradient Descent with Acceleration.

input : $C, \hat{\mathbf{y}}, \text{FOP}, t, \beta$

output: $\alpha^{\text{best}}, \xi^{\text{final}}$

$k = 0, \mathcal{S}^k \leftarrow \emptyset, \alpha^{(k)} \leftarrow \frac{1}{\kappa} \mathbf{1};$

$\mathbf{y}^{(k)} \leftarrow \text{FOP}(\alpha^{(k)});$

$\xi_{\text{ABS}} \leftarrow \alpha^{(k)\top} C \hat{\mathbf{y}} - \alpha^{(k)\top} C \mathbf{y}^{(k)};$

while *True* **do**

$k \leftarrow k + 1;$

$\mathcal{S}^k \leftarrow \mathcal{S}^{k-1} \cup \mathbf{y}^{(k-1)};$

$\alpha^{(k)} \leftarrow \alpha^{(k-1)} - t(C(\hat{\mathbf{y}} - \mathbf{y}^{(k-1)})) + \beta(\alpha^{(k-1)} - \alpha^{(k-2)});$

$\alpha^{(k)} \leftarrow \text{proj}_{\Delta\kappa}(\alpha^{(k)});$

$\mathbf{y}^{(k)} \leftarrow \text{FOP}(\alpha^{(k)});$

if $\alpha^{(k)} = \alpha^{(k-1)}$ **or** $\alpha^{(k)\top} C \hat{\mathbf{y}} - \alpha^{(k)\top} C \mathbf{y}^{(k)} > \xi_{\text{ABS}} + (\alpha^{(k)} - \alpha^{(k-1)})^\top (C(\hat{\mathbf{y}} - \mathbf{y}^{(k-1)}))$ **and**

$\mathbf{y}^{(k)} \in \mathcal{S}^k$ **then**

$\alpha^{\text{final}}, \xi^{\text{final}} \leftarrow \text{GIO}_{\text{ABS}}(\hat{\mathbf{y}}, \mathcal{S}^k);$

$k \leftarrow k + 1;$

$\mathbf{y}^{(k)} \leftarrow \text{FOP}(\alpha^{\text{final}});$

if $\alpha^{\text{final}\top} C \hat{\mathbf{y}} - \alpha^{\text{final}\top} C \mathbf{y}^{(k)} = \xi^{\text{final}}$ **then**

 | **stop**

else

 | $\alpha^{(k)} \leftarrow \alpha^{\text{final}};$

 | $\mathcal{S}^k \leftarrow \mathcal{S}^{k-1} \cup \mathbf{y}^{(k-1)};$

 | $t \leftarrow \frac{t}{2};$

end

else

 | $\xi_{\text{ABS}} \leftarrow \alpha^{(k)\top} C \hat{\mathbf{y}} - \alpha^{(k)\top} C \mathbf{y}^{(k)};$

end

end

end

Algorithm 5: Frank-Wolfe Generalized Inverse Method, Absolute Gap

```

input :  $C, \hat{\mathbf{y}}, \text{FOP}$ 
output:  $\alpha^{\text{final}}, \xi^{\text{final}}$ 
 $k = 0, \mathcal{S}^k \leftarrow \emptyset, \alpha^{(k)} \leftarrow \frac{1}{K} \mathbf{1};$ 
 $\mathbf{y}^{(k)} \leftarrow \text{FOP}(\alpha^{(k)});$ 
 $\xi_{\text{abs}} \leftarrow \alpha^{(k)\top} C \hat{\mathbf{y}} - \alpha^{(k)\top} C \mathbf{y}^{(k)};$ 
while True do
   $k \leftarrow k + 1;$ 
   $\mathcal{S}^k \leftarrow \mathcal{S}^{k-1} \cup \mathbf{y}^{(k-1)};$ 
   $i \leftarrow \arg \min_i C_i (\hat{\mathbf{y}} - \mathbf{y}^{(k-1)});$ 
   $\alpha^{(k)} \leftarrow \alpha^{(k-1)} - \frac{2}{2+k} (\mathbf{e}_i - \alpha^{(k-1)});$ 
   $\mathbf{y}^{(k)} \leftarrow \text{FOP}(\alpha^{(k)});$ 
  if  $\alpha^{(k)} = \alpha^{(k-1)}$  or  $\alpha^{(k)\top} C \hat{\mathbf{y}} - \alpha^{(k)\top} C \mathbf{y}^{(k)} > \xi_{\text{ABS}} + (\alpha^{(k)} - \alpha^{(k-1)})^\top (C(\hat{\mathbf{y}} - \mathbf{y}^{(k-1)}))$  and
     $\mathbf{y}^{(k)} \in \mathcal{S}^k$  then
       $\alpha^{\text{final}}, \xi^{\text{final}} \leftarrow \text{GIO}_{\text{ABS}}(\hat{\mathbf{y}}, \mathcal{S}^k);$ 
       $k \leftarrow k + 1;$ 
       $\mathbf{y}^{(k)} \leftarrow \text{FOP}(\alpha^{\text{final}});$ 
      if  $\alpha^{\text{final}\top} C \hat{\mathbf{y}} - \alpha^{\text{final}\top} C \mathbf{y}^{(k)} = \xi^{\text{final}}$  then
        | stop
      else
        |  $\alpha^{(k)} \leftarrow \alpha^{\text{final}};$ 
        |  $\mathcal{S}^k \leftarrow \mathcal{S}^{k-1} \cup \mathbf{y}^{(k-1)};$ 
      end
    else
      |  $\xi_{\text{ABS}} \leftarrow \alpha^{(k)\top} C \hat{\mathbf{y}} - \alpha^{(k)\top} C \mathbf{y}^{(k)};$ 
    end
  end
end

```

Algorithm 6: Frank-Wolfe Incomplete FOP Solve Subalgorithm, Concurrent MIP Approach, Absolute Gap

input : FOP, \mathbf{C} , $\boldsymbol{\alpha}$, \mathbf{y}^0

output: i , \mathbf{y}

for $i \in 1 \dots \mathcal{K}$ **do**

 | FOP _{i} \leftarrow FOP \cap $\{C_i(\mathbf{y} - \mathbf{y}^0) \leq C_j(\mathbf{y} - \mathbf{y}^0) \mid j \in 1 \dots \mathcal{K} \setminus i\}$;

end

$u \leftarrow \infty$;

$p \leftarrow \mathcal{K}$;

$\forall i$, concurrently initiate optimizing FOP _{i} with objective coefficients $\boldsymbol{\alpha}$;

while FOP _{i} is solving **do**

 | **if** FOP _{i} .upper_bound $<$ u **then**

 | $u \leftarrow$ FOP _{i} .upper_bound;

 | **end**

 | **if** FOP _{i} .lower_bound $>$ u **then**

 | $p \leftarrow p - 1$;

 | terminate FOP _{i} ;

 | **end**

 | **if** $p = 1$ **then**

 | $\mathbf{y} \leftarrow$ incumbent solution of FOP _{i} ;

 | terminate FOP _{i} ;

 | **return** i , \mathbf{y}

 | **end**

end

Algorithm 7: Frank-Wolfe Partial FOP Inverse Method

```

input :  $\mathbf{C}, \hat{\mathbf{y}}, \text{FOP}$ 
output:  $\boldsymbol{\alpha}^{\text{final}}, \xi^{\text{final}}$ 
 $k = 0, \mathcal{S}^k \leftarrow \emptyset, \boldsymbol{\alpha}^{(k)} \leftarrow \frac{1}{\kappa} \mathbf{1};$ 
 $i, \mathbf{y}^{(k)} \leftarrow \text{Alg7}(\text{FOP}, \mathbf{C}, \boldsymbol{\alpha}^{(k)}, \hat{\mathbf{y}});$ 
 $\xi_{\text{ABS}} \leftarrow \boldsymbol{\alpha}^{(k)\top} \mathbf{C} \hat{\mathbf{y}} - \boldsymbol{\alpha}^{(k)\top} \mathbf{C} \mathbf{y}^{(k)};$ 
while True do
   $k \leftarrow k + 1;$ 
   $\mathcal{S}^k \leftarrow \mathcal{S}^{k-1} \cup \mathbf{y}^{(k-1)};$ 
   $\boldsymbol{\alpha}^{(k)} \leftarrow \boldsymbol{\alpha}^{(k-1)} - \frac{2}{2+k} (\mathbf{e}_i - \boldsymbol{\alpha}^{(k-1)});$ 
   $i, \mathbf{y}^{(k)} \leftarrow \text{Alg7}(\text{FOP}, \mathbf{C}, \boldsymbol{\alpha}^{(k)}, \hat{\mathbf{y}});$ 
  if  $\boldsymbol{\alpha}^{(k)} = \boldsymbol{\alpha}^{(k-1)}$  or  $\boldsymbol{\alpha}^{(k)\top} \mathbf{C} \hat{\mathbf{y}} - \boldsymbol{\alpha}^{(k)\top} \mathbf{C} \mathbf{y}^{(k)} > \xi_{\text{ABS}} + (\boldsymbol{\alpha}^{(k)} - \boldsymbol{\alpha}^{(k-1)})^\top (\mathbf{C}(\hat{\mathbf{y}} - \mathbf{y}^{(k-1)}))$  and
     $\mathbf{y}^{(k)} \in \mathcal{S}^k$  then
       $\boldsymbol{\alpha}^{\text{final}}, \xi^{\text{final}} \leftarrow \text{GIO}_{\text{ABS}}(\hat{\mathbf{y}}, \mathcal{S}^k);$ 
       $k \leftarrow k + 1;$ 
       $\mathbf{y}^{(k)} \leftarrow \text{FOP}(\boldsymbol{\alpha}^{\text{final}});$ 
      if  $\boldsymbol{\alpha}^{\text{final}\top} \mathbf{C} \hat{\mathbf{y}} - \boldsymbol{\alpha}^{\text{final}\top} \mathbf{C} \mathbf{y}^{(k)} = \xi^{\text{final}}$  then
        stop
      else
         $\boldsymbol{\alpha}^{(k)} \leftarrow \boldsymbol{\alpha}^{\text{final}};$ 
         $\mathcal{S}^k \leftarrow \mathcal{S}^{k-1} \cup \mathbf{y}^{(k-1)};$ 
         $t \leftarrow \frac{t}{2};$ 
      end
    else
       $\xi_{\text{ABS}} \leftarrow \boldsymbol{\alpha}^{(k)\top} \mathbf{C} \hat{\mathbf{y}} - \boldsymbol{\alpha}^{(k)\top} \mathbf{C} \mathbf{y}^{(k)};$ 
    end
  end
end

```

Algorithm 8: Boosted Coarsening Ensemble Generation Method

input : $G = \{V, E\}$, n , η **output:** \mathbb{G} $\mathbb{G} \leftarrow \{\}$; $\mathbf{w}_e \leftarrow 1, \quad \forall e \in E$;**for** $i \in \text{range}(n)$ **do** $\mathbf{o}_e \leftarrow \mathbf{w}_e \text{Exp}(\lambda = 1), \quad \forall e \in E$; $O \leftarrow [e \in E \mid \mathbf{o} \text{ sorted in ascending order}]$; $\mathcal{C} \leftarrow \{\}$; **for** $e = (v_1, v_2) \in O$ **do** **if** $\exists c \in \mathcal{C} \mid v_1 \in c \text{ or } v_2 \in c$ **then** $\mathbf{w}_e \leftarrow \eta \mathbf{w}_e$ **else** $\mathcal{C} \leftarrow \mathcal{C} \cup e$; $\mathbf{w}_e \leftarrow \frac{\mathbf{w}_e}{\eta}$ **end** **end** $G' \leftarrow G$; contract all edges e of G' where $e \in \mathcal{C}$; $\mathbb{G} \leftarrow \mathbb{G} \cup G'$ **end**

Algorithm 9: Projected gradient descent method with stochastic subgradient estimation.

input : $C, \hat{\mathbf{y}}, \text{FOP}, t, n_k, K$
output: $\boldsymbol{\alpha}^{\text{best}}$
 $k = 0, \mathcal{S}^k \leftarrow \emptyset, \boldsymbol{\alpha}^{(k)} \leftarrow \frac{1}{K} \mathbf{1};$
for $i \in 1 \dots n_k$ **do**
 $\text{FOP}_i \leftarrow \text{Coarsen}(\text{FOP});$
 $\mathbf{y}_i^{(k)} \leftarrow \text{FOP}_i(\boldsymbol{\alpha}^{(k)});$
end
 $\mathbf{y}^{(k)} \leftarrow \arg \min_{\mathbf{y}_i^{(k)}} \boldsymbol{\alpha}^{(k)\top} \mathbf{C} \mathbf{y}_i^{(k)};$
 $\xi_{\text{ABS}} \leftarrow \boldsymbol{\alpha}^{(k)\top} \mathbf{C} \hat{\mathbf{y}} - \boldsymbol{\alpha}^{(k)\top} \mathbf{C} \mathbf{y}^{(k)};$
while $k < K$ **do**
 $k \leftarrow k + 1;$
 $\mathcal{S}^k \leftarrow \mathcal{S}^{k-1} \cup \mathbf{y}^{(k-1)};$
 $\boldsymbol{\alpha}^{(k)} \leftarrow \boldsymbol{\alpha}^{(k-1)} - t(\mathbf{C}(\hat{\mathbf{y}} - \mathbf{y}^{(k-1)}));$
 $\boldsymbol{\alpha}^{(k)} \leftarrow \text{proj}_{\Delta^{\mathcal{K}}}(\boldsymbol{\alpha}^{(k)});$
for $i \in 1 \dots n_k$ **do**
 $\text{FOP}_i \leftarrow \text{Coarsen}(\text{FOP});$
 $\mathbf{y}_i^{(k)} \leftarrow \text{FOP}_i(\boldsymbol{\alpha}^{(k)});$
end
 $\mathbf{y}^{(k)} \leftarrow \arg \min_{\mathbf{y}_i^{(k)}} \boldsymbol{\alpha}^{(k)\top} \mathbf{C} \mathbf{y}_i^{(k)};$
 $\xi_{\text{ABS}} \leftarrow \boldsymbol{\alpha}^{(k)\top} \mathbf{C} \hat{\mathbf{y}} - \boldsymbol{\alpha}^{(k)\top} \mathbf{C} \mathbf{y}^{(k)};$
end

$$\boldsymbol{\alpha}^{\text{best}} \leftarrow \frac{\sum_{i \in 0 \dots K} (i+1)^2 \boldsymbol{\alpha}^{(i)}}{\sum_{i \in 0 \dots K} (i+1)^2};$$
stop;
